International Journal of Concrete Structures and Materials

RESEARCH Open Access

Utilization of Various Industrial Wastes in Ordinary Concrete Under Normal Manufacturing Conditions

Sherif H. Al-Tersawy[1], Sahar E. Zakey[1], Rasha A. El-Sadany[2] and Hossam El-Din M. Sallam[3*]

Abstract

The main objective of the present work is to evaluate using alkaline wastewater from pot factories (recycled NaOH solutions with variant concentrations and pH values) along with waste powders possessing pozzolanic properties, such as supplementary cementitious materials and stone waste dust in concrete under normal manufacturing conditions. An extensive analysis of the chemical components and the physical properties of the used materials was achieved. Both supplementary cementitious materials and stone waste dust materials were used as 0%, 10%, 20%, or 30% partial cement replacements using either tap water or alkaline wastewater to make samples for physical, mechanical, and microstructure testing. Thermodynamic modeling was used to evaluate the effect of the flushed alkaline industrial water and the powders on the hydration products. The results showed an increase in the workability of the mixes made with alkaline wastewater, an increase in water absorption for samples made with alkaline wastewater at the age of 28 days, and a relative decrease in compressive strength at 3 and 28 days, respectively. Despite the reduction in mechanical strength, most samples made with alkaline wastewater and 10%, 20% supplementary cementitious materials, or stone waste dust materials gave an accepted concrete grade. The microstructure analysis showed a slight change in pores distribution, pores values, and hydration products at 3 and 28 days. The thermodynamic analysis provided insight into data on the effect of supplementary cementitious materials, stone waste dust materials, and alkaline wastewater on hydration products. Finally, the combination of these wastes in concrete production showed satisfactory conclusions.

Keywords Alkaline water, Supplementary cementitious materials (SCMs), Stone waste dust materials (SWDs), Physical properties, Mechanical properties, Thermodynamic properties

1 Introduction

Sodium hydroxide (NaOH) residues resulting from utensils factories and carpet and rug factories represent a significant financial burden for treatment before disposal in drainage networks. These residues can be highly corrosive and, if not properly treated, can damage the local water supply and have a negative environmental impact. Additionally, the work of shaping and cutting stones results in a large amount of waste that must be disposed of in an environmentally responsible manner. This waste often fills vast areas of land and requires high costs for disposal in many industrial areas in the world. Proper management of these residues is essential to preventing

Journalinformation: ISSN 1976-0485 / eISSN 2234-1315

*Correspondence:
Hossam El-Din M. Sallam
hem_sallam@zu.edu.eg; hem_sallam@yahoo.com
[1] Civil Engineering Department, Higher Technological Institute (HTI), 10th of Ramadan City 44629, Egypt
[2] Radiation Engineering Department, National Center for Radiation Research and Technology, Egyptian Atomic Energy Authority, Cairo 11787, Egypt
[3] Materials Engineering Department, Zagazig University, Zagazig 44519, Egypt

Springer Open

© The Author(s) 2023. **Open Access** This article is licensed under a Creative Commons Attribution 4.0 International License, which permits use, sharing, adaptation, distribution and reproduction in any medium or format, as long as you give appropriate credit to the original author(s) and the source, provide a link to the Creative Commons licence, and indicate if changes were made. The images or other third party material in this article are included in the article's Creative Commons licence, unless indicated otherwise in a credit line to the material. If material is not included in the article's Creative Commons licence and your intended use is not permitted by statutory regulation or exceeds the permitted use, you will need to obtain permission directly from the copyright holder. To view a copy of this licence, visit http://creativecommons.org/licenses/by/4.0/.

environmental damage and protecting the health of local communities. On the 10th of Ramadan city, an Egyptian industrial city, the treatment and disposal of the NaOH solution after several times of its use represents a burden on manufacturers and the surrounding environment. The environmental effect of NaOH industrial waste as a very high production volume compound has been stated in European Commision, 2006. Although Na is an essential nutrient for living organisms, the effects on the pH value of the aquatic environment are a major concern. Also, adverse effects are due to OH^-. In Ghrair and Al-Mashaqbeh, (2016), mortar and concrete mixes made with secondary treated wastewater from a wastewater treatment plant in Jordan showed no negative impact on compressive strength or soundness value. In an investigation on waste wash water from ready-mix concrete plants with extremely high dissolved solids 9000 mg/L, heavy metals, and extremely alkaline with pH 12, the outcomes of experimental work revealed that when it was used to replace 75% of the mix water, it did not result in statistically significant strength reductions at the 95% confidence level. There were no major implications for workability (Ghrair et al., 2020).

On the other hand, using stone waste dust (SWD) from the ornamental stone industry and supplementary cementitious materials (SCMs) from cement, steel, and industrial production alleviates the environmental burden. Besides the side effects of its uncontrolled dumping, the SWD has been shown to have a detrimental effect on public health (El-Gammal et al., 2011). The effect of SWDs and SCMs on cement pastes has been investigated in some research (Abdel-Gawwad et al., 2019; Kumar et al., 2013; Vollpracht et al., 2016). A reaction prediction approach in conjunction with a strength–heat master curve was used to simulate the hydration of various mixes composed of limestone (LS) as a partial replacement of cement, optimizing the binder proportion (Kumar et al., 2013). The variables included type of cement, LS fineness, and percentage of partial replacement. The effect of SCMs on the pore solution composition of blended cement was reviewed in Vollpracht et al. (2016). The effect of the partial replacement of marble dust (MD) in a cement mortar on the fresh and hardened properties was studied (Abukersh & Fairfield, 2011). The results proved that the best exchange value is 10%. The effect of grinding degrees of CKD up to nano-scales was studied as a partial substitute for cement in cement mortar mixes. The results showed an improvement in compressive strength ranging between 15 and 30% at a CKD replacement ratio of 20% (Bacarji et al., 2013). The analysis demonstrated a decrease in the proportion of Portlandite following the increase in the degree of fineness of CKD and an enhancement of the microstructure due to the improvement of hydration products. An equal volume of MD paste to the cement paste in mortar mixes was replaced (Vijayalakshmi et al., 2013). Using 20% MD paste leads to a 33% decrease in cement content and an increase of 20% in compressive strength at 28 days. However, this percentage of paste replacement leads to a significant increase in superplasticizer dose.

The contribution of SWDs and SCMs to concrete mixes has been studied in many works (Ashish, 2019 Feb; Gudainiyan & Kishore, 2023; Tugrul, 2019). The partial replacement of cement by weight with 30% red granite dust (GD) showed strength results comparable to, or better than, equivalent control mixes (Abukersh & Fairfield, 2011). The effect of the crystalline nature of MD and GD used as a partial cement replacement was investigated. The non-pozzolanic nature of the powder showed no enhancements to the compressive strength up to 5% replacement. The numerical analysis of this work gave a clear correlation between the replacement of these fillers and the resulting compressive strength. MD was used as an additive in conventional, self-compacted, and polymer concrete mixes. The major contribution of MD was noticed in the conventional concrete, while it showed no effect on the other mixes. A comprehensive review of granite waste's use in concrete production was made as a partial aggregate or cement replacement (Arel & Shaikh, 2019). When granite waste was used as a fine aggregate partial replacement, the best mechanical performance was achieved at a ratio equal to or less than 15%. When GD was used as a partial cement replacement, the best mechanical performance was achieved at a ratio equal to or less than 5%. The workability of concrete made with granite waste as a partial replacement for aggregate was adversely affected. In an interesting review (Tugrul, 2019), correlation equations were proposed to predict the compressive and tensile strength of concrete containing marble waste as a partial replacement of sand or cement. The durability of cementitious materials with SWDs and SCMs was discussed in some studies (Lauermannová et al., 2020; Taji et al., 2019; Zajac et al., 2018). Several types of research have been done on using coarse waste aggregates in concrete (McNeil & Kang, 2013). In these studies, the mechanical performance of different types of coarse aggregate was observed, with some results showing improved mechanical performance compared to natural coarse aggregate (Tugrul Tunc & Alyamac 2020; Tugrul Tunc & Esat, 2019).

Although many studies (L'Hôpital et al., 2016; Shi & Lothenbach, 2020; Weerdt et al., 2019) have proved the usefulness of thermodynamic equilibrium models for describing cement hydration, the success and accuracy of these results depend on a reliable thermodynamic database (Abzaev et al., 2019; Kunther et al., 2016; Shi

& Lothenbach, 2019). Thermodynamic and thermodynamic software became crucial to understanding the fundamental connections between composition and the formed hydrates for a certain mix composition. Hence, predicting their mechanical and durability aspects could be achieved (Fernández et al., 2018; Lothenbach & Zajac, 2019; Prentice et al., July 2018). Some related research works found (El-Dieb et al., 2019; Jhatial et al., 2023; Liu et al., xxxx) that using some SCMs, such as BFS and CD, as a part of cementitious materials significantly reduces the hydration temperature in the early ages. Also, the relatively late reaction of these materials contributes to obtaining almost rewarding mechanical properties for the control samples. It was found that these substances' activation can be done to ensure their full activity in the reaction.

The most commonly used recycled materials are cementitious materials with pozzolanic action, such as cement kiln dust and blast furnace slag powders. Other materials, such as granite, marble, and limestone dust, are also used as fillers. These recycled materials can help reduce the amount of cement used and improve strength, durability, and workability. They are also more sustainable and cost-effective, making them an ideal choice for use in the manufacture of concrete (Arel & Shaikh, 2019 Feb 1; Tugrul, 2019; Vollpracht et al., 2016). On the other hand, several studies (Gudainiyan & Kishore, 2023) showed that properly processed agricultural waste materials make them suitable to replace cement in concrete production due to their pozzolanic properties. It can be noted that only some research studies the effect of wastewater as mixing water along with waste powders as a partial replacement of cement in concrete manufacturing. Therefore, this study aims to fill this research gap and investigate the effect of this combination on fresh and hard concrete properties.

2 Research Significance

In an industrial city such as the 10th of Ramadan, Egypt, several factories produce tons of alkaline water a year while others produce massive amounts of stone waste powder such as marble and granite. Investigating the individual and combined effect of the recycled NaOH solutions with variant concentrations and pH values, SWDs, and SCMs wastes in the concrete work under the normal cast and curing conditions would contribute to alleviating the burden on the surrounding environment and reducing the economic cost of the construction process as well. Therefore, this study used three industrial waste categories to produce concrete under normal manufacturing (cast-curing) conditions. The first category used alkaline wastewater (AW) from pot factories (recycled NaOH solutions with variant concentrations and pH values) as mixing water. Secondly, SCMs from cement and steel factories, namely cement kiln dust and blast furnace slag, have partially replaced cement. Finally, SWDs from ornamental works, including granite, marble, and limestone dust, have partially replaced cement.

3 Experimental Program

The objective of the practical program of this research was to examine the effect of replacing parts of cement with proportions of 10, 20, and 30% by weight with types of SCMs (CD and BFS), as well as types of SWDs (MD, GD, and LS dust) on the workability properties, voids ratio, as well as the mechanical properties of concrete at the age of 28 days. Most recycled cementitious materials used to replace cement in concrete production do not exceed 30% because these materials are not as strong or durable as conventional cement. They cannot replace more than 30% of the cement in concrete production without compromising the strength and durability of the concrete. The 0–30% range is safe to use to ensure that the concrete produced is still strong and durable despite using recycled materials (Abukersh & Fairfield, 2011; El-Dieb et al., 2019; Jhatial et al., 2023). Samples of cement pastes were made using the same materials to examine the microstructure of the hardened pastes by taking SEM photos. The samples were made using ordinary drinking water that follows the specifications of mixing water for concrete as well as alkaline water from a pots factory in Badr city (Fig. 1). A chemical analysis of cement and replacement materials, whether they were SCMs, MD, GD, and LS dust, was done as well as a chemical analysis of the alkaline water used in the experiments. TEM images were taken to determine the mean size of the stone powder grains' diameters. For concrete materials of fine aggregate or coarse aggregate, physical and mechanical tests were carried out. The considered materials were used to make normal stress concrete mixtures to study the operability properties of fresh concrete and hardened concrete's physical and mechanical properties. Concrete contained different substitution ratios of cement materials, such as cement powder and iron furnace slag powder, as well as the same substitution ratios of marble, granite, and limestone powder. The results of the chemical analysis of materials were used as the main inputs in the theoretical study using the thermodynamics model.

3.1 Materials

3.1.1 SCMs and SWDs Materials

Table 1 shows the chemical composition of cement, SCMs, and SWDs materials. The materials used as SCMs included blast furnace slag (BFS) and cement kiln dust (CKD), while the SWDs included granite dust (GD), marble dust (MD), and limestone dust (LS). The

Fig. 1 Pots washing machine using NaOH solution in Nouval factory, Badr city

Table 1 Chemical composition of cement, BFS, CKD, GD, MD, and LS

Oxide	Cement	SCMs		SWDs		
		BFS	CKD	GD	MD	LS
SiO_2	19.51	12.52	5.01	62.47	22.47	0.83
TiO_2	0.39	0.36	0.12	0.63	0.25	0.02
Al_2O_3	3.94	7.27	2.00	10.55	5.13	0.15
Fe_2O_3	4.33	30.78	2.66	3.15	3.06	0.37
MnO	0.20	2.72	0.13	0.05	0.07	0.02
MgO	2.43	3.55	1.18	0.65	1.24	5.02
CaO	58.97	26.39	44.07	8.36	39.69	48.26
Na_2O	0.62	0.59	1.36	4.46	1.38	0.18
K_2O	0.22	0.12	3.99	3.70	1.11	0.04
P_2O_5	0.11	0.40	0.03	0.34	0.17	0.04
SO_3	5.21	1.08	4.15	0.17	0.59	0.33
Cl	0.11	0.34	5.51	0.05	0.22	0.19
ZnO	0.03	0.58	0.01	0.03	0.01	0.02
Cr_2O_3	0.03	1.15	0.00	0.03	0.01	0.02
BaO	0.00	0.19	0.00	0.09	0.00	0.02
CuO	0.00	0.11	0.01	0.00	0.01	0.00
LOI	3.54	11.55	29.70	5.28	24.46	44.42
Sum	99.63	99.69	99.92	100.00	99.87	99.93

CKD was brought from the Suez cement factory, and the BFS was brought from Elmasreen Factory for steel industries. The stone waste powders were brought from ornamental stone factories in the two industrial cities (10^{th} of Ramadan and Badr cities). Chemical analyses of these materials as alkaline wastewater were performed at the National Research Center (NRC), Cairo, Egypt. Fig 2 shows a sample of BFS, CKD, GD, MD, LS.

Image analysis of SWDs powder and CKD powder proved their fineness due to the electric saw-cutting process during the various shaping operations in stone factories. The size of most of the powder particles used was in the range of (7.5–112 nm) as was proven by TEM images (Fig. 3). As it was deduced earlier (Li et al., 2019) and as a result of Mohr's number being in the range of 3, the LS and MD powders are much softer than cement. On the other hand, the raw BFS powder was of higher

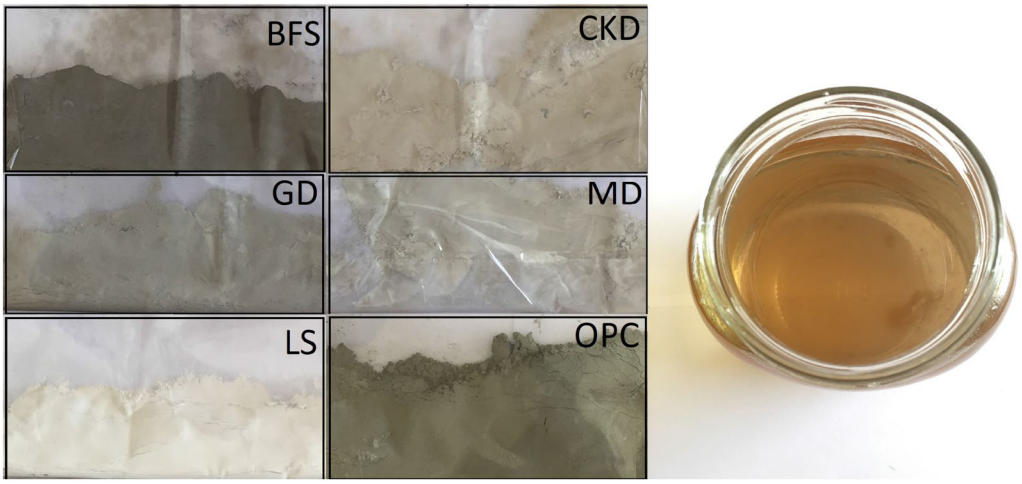

Fig. 2 Samples of BFS, CKD, GD, MD, LS, OPC, and AW

roughness due to the different manipulation processes. Thus, the powder was prepared before use by drying it in the oven at a temperature of 100°c for one hour and then was sieved on a standard 90 µm. The passed powder was used in the practical program to neutralize the effect of the fineness of both SCMs and SWDs powders on either the chemical reactions in the case of relatively active powders (SCMs) or the effect of fineness as a filler in the case of SWDs.

3.1.2 Alkaline Water

Table 2 shows the waste alkaline water (AW) chemical analysis. The water was brought from the Nouval factory in Badr city. The AW was collected at the end of life (disposal stage) from the drainage system of the machine shown in Fig. 1. The AW was kept at room temperature in a sealed container and was tested shortly after collection in the XRF labs of NRC. Fig 2 shows a sample of AW.

3.1.3 Cement and Aggregates

Ordinary Portland cement from the Suez cement company in Egypt was used. The type of cement was CEM I 42.5 N. Tests were carried out on the cement, according to ESS 2421, (2005). The cement test results considering fineness, setting, soundness, and strength, were conducted in the NRC materials lab and showed suitability for concrete works (Table 3). Aggregates were brought from local Egyptian sources and consisted of gravel with a nominal maximum size of 10 mm and medium-fine sand. The physical and mechanical properties were made according to ESS (1109), 2002. Table 4 shows the results.

3.2 Samples and Procedures

3.2.1 Concrete Samples

The experimental work aimed to design, prepare, cast, and test 16 mixes of concrete using tap water (Series 1-TW) that is suitable for concrete mixing and a similar 16 mix of concrete using alkaline water (Series 2-AW) with a composition as prescribed in Table 2. Each series consisted of a control mix and 15 concrete mixes divided into five cement replacement powder types: BFS, CKD, GD, MD, and LS. Each type included three replacement ratios of 10%, 20%, and 30%, as listed in Table 5. The water–cement ratio (w/c) was kept constant in all mixes and equal to 0.4. A water reducer with a percentage of 2% cement weight was used to get a suitable and even consistency for all mixes. The resulting slump for all mixes was in the range (of 25–35) mm. The prescribed mixes were used to cast samples of cubes (10×10 cm) and cubes (15×15 cm) to determine absorption and compressive strength. The compressive strength and absorption ratio were determined by considering the average of three tested cubes from each mix as the mean value according to ESS 1658, (2006).

3.2.2 Microstructure Samples

Small samples of cement pastes with either SCMs or SWDs were cast to study the microstructure using SEM images. A small cylindrical mold with a 2.8 cm inner diameter and 3 cm height was used to cast the paste samples (Fig. 4). The purpose of making samples of paste was to control well the conditions surrounding the chemical reactions to take accurate backscattered (BSE) SEM images that contain the variables needed to analyze and determine microstructure elements

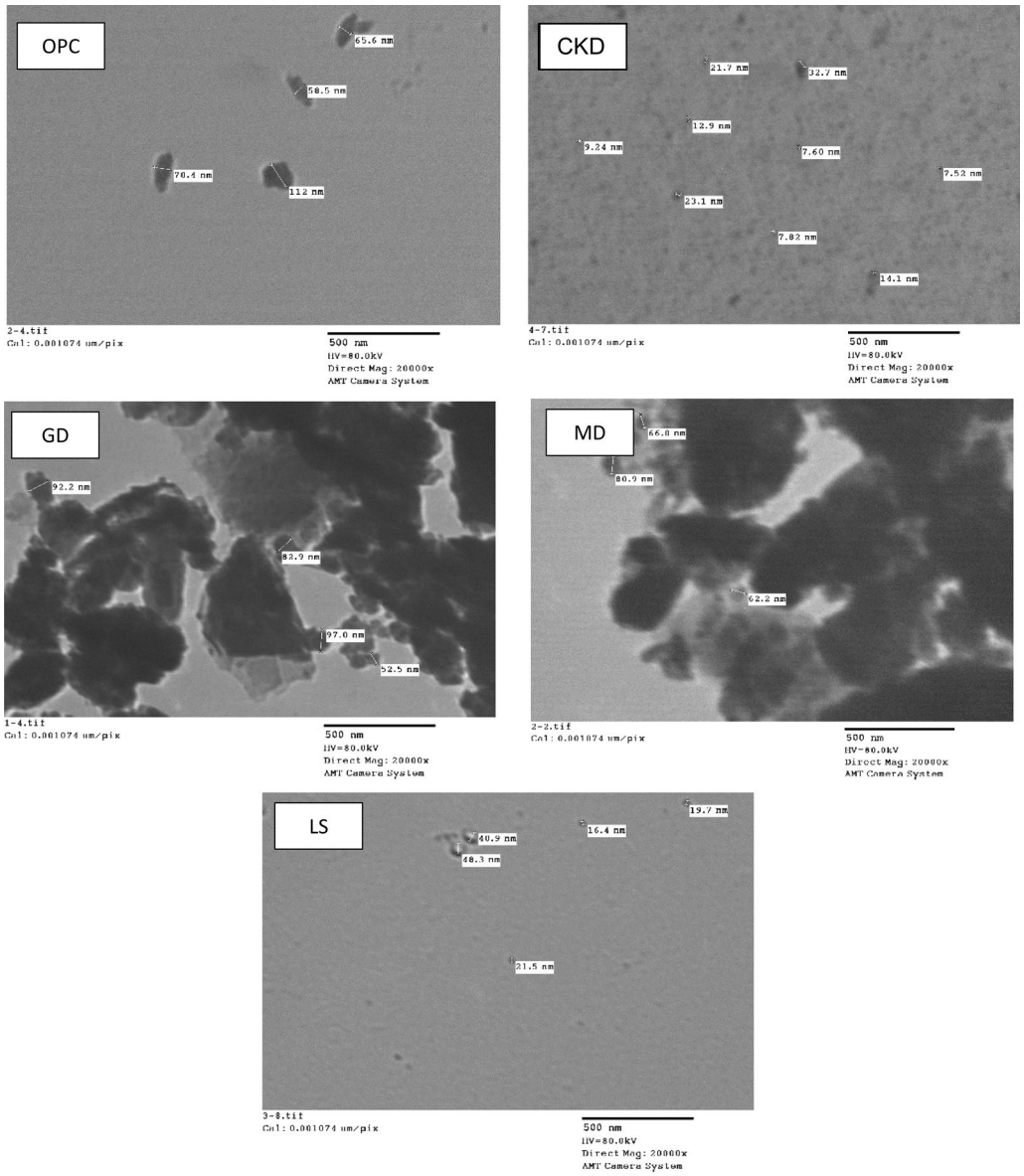

Fig. 3 TEM images for SCMs and SWDs powders

Table 2 Chemical composition of alkaline water (AW)

Test	Amount
Cl (ppm)	56
SO_3 (ppm)	90
TDS (ppm)	3100
Organic materials (ppm)	160
CO_3 (ppm)	300
HCO_3 (ppm)	1365
TSS (ppm)	16
NaOH (ppm)	176
pH	9.06

Table 3 Mechanical properties of cement

Properties	Measured values
Blaine surface area (cm^2/gm)	2800
Soundness (Le Chatelier) (mm)	1.1
Initial setting time (min)	115
Final setting time (min)	180
Compressive strength (MPa)	
7 days	23
28 days	51

Table 4 Properties of gravel and sand

Test	Gravel	Sand
Specific weight	2.56	2.61
Bulk density (t/m^3)	1.65	1.75
Clay and fine dust content (%)	1.6	1.5
Abrasion (Los Angeles) (%)	12.7	–
Water absorption	1.1	–
Impact value (%)	11.1	–

accurately and also to find a common base for comparison and evaluation of the results of thermodynamic analysis, which adopts the same components and the same mixing ratios. A total of 14 samples were cast in two sets. The first set was made with TW, while the second set was made using AW, and each one included: Control, 10% CKD, 20% CKD, 10% BFS, 20% BFS, 10% LS, and 20% LS. For each sample, the image was taken at 3 and 28 days at two specified magnifications of 350 and 2000 times with a total SEM image of 54.

The scanning electron microscope type was (SEM, Joel-JXA-840A) and digital imaging; X-ray diffractometer (XRD, Philips Analytical X-ray B.V. Machine). The BSE images allow the prediction of pores and hydrated ratios using grey colors as an identification method which can be made using image processing software (2021b; Al-Tersawy et al., 2021).

3.2.3 Thermodynamics Modeling

Since even common hydrated ordinary Portland cement contains at least seven hydrates, thermodynamic modeling of such a multicomponent-multiphase system and experiments in the same context allow an understanding of the effect of different parameters involved, the reaction mechanisms, and the final outputs.

Based on the composition of the starting materials and hydration time, the phase assemblage can be easily predicted through thermodynamic calculations based on a valid database for any geochemical system. The thermodynamic calculations determine which solids and solutions are stable under the input conditions, and all chemical reactions among solids, solid solutions, gaseous phase, and aqueous electrolytes are considered (Lothenbach & Zajac, 2019).

The available thermodynamic codes depend on two basic approaches to solving the geochemical equilibrium problem:

- Solving the law of mass action (LMA) equations.
- Minimizing the Gibbs free energy of the system.

GEMS (Kulik et al., 2013) presents the Gibbs free energy approach and has the advantage that no prior assumptions must be made. GEMS implements a thermodynamic approach to quantify the contents of hydration products and pH value description over a long period. In that phase, the composition of solid solutions, pH, redox potential, and the fugacity of gases is obtained as an output parameter.

GEMS uses thermodynamic parameters at the consecutive stages of cement hardening to get the Gibbs free energy by considering an incremental balance between the dissolution rate of clinker phases and the deposition of solid solutions of individual phases. The refined experimental equations used are as follows (Lothenbach et al., 2008):

$$R_{t,T} = fracK_1N_1.(1-\alpha_t).\left(-ln(1-\alpha_t)^{1-N_1}\right) \cdot\left(\frac{rh-0.55}{0.45}\right)^4.\frac{S}{385}\exp\left(-\frac{E_a}{R}\left(\frac{1}{T}-\frac{1}{T_0}\right)\right) \quad (1)$$

$$R_{t,T} = \frac{K_1.(1-\alpha_t)^{2/3}}{1-(1-\alpha_t)^{1/3}}.\left(\frac{rh-0.55}{0.45}\right)^4\exp\left(-\frac{E_a}{R}\left(\frac{1}{T}-\frac{1}{T_0}\right)\right), \quad (2)$$

$$R_{t,T} = K_3.(1-\alpha_t)^{N_3}.\left(\frac{rh-0.55}{0.45}\right)^4\exp\left(-\frac{E_a}{R}\left(\frac{1}{T}-\frac{1}{T_0}\right)\right), \quad (3)$$

where rh is the degree of the system closing (e.g., $rh=1$ when the system is closed); E_s is the activation energy of dissolution; T and T_0 are current and room temperature, respectively; S is the surface area of the phase nucleus; α_t is the degree of hydration which can be obtained from the following:

$$\alpha_t = \alpha_{t-1} + \Delta t.R_{t-1}[1+3.333.(H\mu-\alpha_t)]^4, \quad (4)$$

where μ is the w/c, the hydration process develops when $(H\mu\text{-}\alpha_t)<0$; K_1, N_1, K_2, K_3, N_3, and H are parameters of the Parrot, Killoh and Lothenbach model and given in Table 6. Table 7 shows Bogue's values of the ordinary Portland cement used. The order of Eqs. (1–3) describes the incremental development of cement hydration until the final stable stage considering w/c, humidity, and specific surface of phase nuclei. This development is in the following order: Stage 1 is the nucleation and development of phases. Stage 2 is diffusion processes, where phenomenological dependences of reaction rates and hydration parameters are obtained for each clinker phase. Stage 3, hydration degree (Abzaev et al., 2019). The reactions of the SCMc during the input stage were restricted to 75% and 50% for BFS and CKD, respectively (El-Dieb et al., 2019; Fernández et al., 2018).

Table 5 Groups, mixes, mixes quantities, and results

Mix	Description	Cement (400 kg/m^3)	Gravel (1225 kg/m^3)	Sand (612.5 kg/m^3)	TW or AW (160/m^3)	WR (2 L/100 kg of cement)	Dust amount (kg)	Slump (cm)		Density (t/m^3)		% Absorption (28 days)	
								TW	AW	TW	AW	TW	AW
C	Control (%)	6.04	18.5	9.2	2.4	0.12	–	3.5	4.4	2.257	2.262	4.55	5.14
SCMc													
CKD	10	5.44	18.5	9.2	2.4	0.12	0.54	3.6	4.3	2.262	2.267	4.90	5.31
	20	4.83	18.5	9.2	2.4	0.12	0.97	3.4	4.4	2.267	2.261	4.30	4.68
	30	4.23	18.5	9.2	2.4	0.12	1.27	3.4	4.3	2.271	2.276	4.15	4.20
BFS	10	5.50	18.5	9.2	2.4	0.12	0.54	3.3	4.0	2.259	2.255	2.60	2.84
	20	5.07	18.5	9.2	2.4	0.12	0.97	3.2	3.8	2.262	2.257	4.70	4.87
	30	4.77	18.5	9.2	2.4	0.12	1.27	3.1	3.6	2.264	2.270	9.80	10.62
SWDs													
GD	10	5.50	18.5	9.2	2.4	0.12	0.54	3.3	4.1	2.263	2.268	5.06	5.72
	20	5.07	18.5	9.2	2.4	0.12	0.97	2.9	4.0	2.269	2.264	3.94	4.20
	30	4.77	18.5	9.2	2.4	0.12	1.27	2.7	3.8	2.275	2.270	3.80	3.92
MD	10	5.50	18.5	9.2	2.4	0.12	0.54	3.4	4.1	2.263	2.269	5.50	6.50
	20	5.07	18.5	9.2	2.4	0.12	0.97	3.3	4.3	2.270	2.275	4.10	4.61
	30	4.77	18.5	9.2	2.4	0.12	1.27	3.1	4.1	2.276	2.271	4.00	4.50
LS	10	5.50	18.5	9.2	2.4	0.12	0.54	3.3	4.3	2.262	2.257	4.90	5.70
	20	5.07	18.5	9.2	2.4	0.12	0.97	3.2	4.3	2.266	2.272	5.40	5.85
	30	4.77	18.5	9.2	2.4	0.12	1.27	3.2	4.3	2.271	2.277	5.70	5.95

Mix	Comp. strength (N/mm^2)								Pores %-28 days-BSE		Hydrates %			
	TW				AW						BSE-28 days		GEMS-1000 days	
	3-Days	SD	28-Days	SD	3-Days	SD	28-Days	SD	TW	AW	TW	AW	TW	AW
C	12.38	1.14	30.95	2.33	12.27	2.45	29.69	2.10	0.14	0.17	52.00	39.75	47.30	47.24
SCMc														
CKD	12.59	0.81	30.21	1.37	11.35	2.78	27.58	2.20	0.15	0.24	51.20	38.60	45.86	45.42
	9.82	2.14	25.52	2.58	10.09	0.53	24.72	3.10	0.26	0.25	48.00	45.35	43.94	43.42
	9.89	2.77	25.01	2.45	9.25	2.58	23.12	0.04	–	–	–	–	41.69	41.28
BFS	11.88	2.33	30.54	0.53	11.95	1.11	28.67	2.78	0.15	0.20	55.10	42.00	47.45	46.81
	11.61	2.86	28.44	1.11	9.98	2.20	25.66	0.34	0.14	0.24	53.90	39.00	46.99	46.33
	9.34	1.37	23.08	0.53	9.19	2.04	23.89	1.14	–	–	–	–	45.91	45.18
SWDs														
GD	12.74	1.55	32.73	1.41	12.57	0.53	30.30	1.55	–	–	–	–	–	–
	12.82	0.53	33.33	0.99	12.21	3.10	29.07	1.19	–	–	–	–	–	–
	10.38	0.12	25.12	2.77	9.23	1.97	23.91	1.97	–	–	–	–	–	–
MD	12.81	1.41	30.87	2.54	10.66	0.34	27.72	2.14	–	–	–	–	–	–
	12.48	0.81	29.69	2.86	9.77	2.10	24.90	0.81	–	–	–	–	–	–
	9.14	0.04	23.29	1.46	10.28	1.46	25.40	2.04	–	–	–	–	–	–
LS	11.11	0.34	26.99	0.97	9.25	2.78	24.23	2.78	0.31	0.33	37.00	41.40	35.44	45.11
	10.35	2.80	26.81	1.89	9.26	1.89	23.44	2.80	0.45	0.47	45.00	39.50	42.51	40.80
	8.81	2.54	23.08	0.53	8.95	0.97	23.00	0.12	–	–	–	–	30.28	36.77

Fig.4 Paste samples for microstructure examination

Table 6 Parameters of Parrot, Killoh, and Lothenbach

Parameter	Alite	Belite	Aluminate	Ferrite
K_1	1.5	0.5	1	0.37
N_1	0.7	1	0.85	0.7
K_2	0.05	0.006	0.04	0.015
K_3	1.1	0.2	1	0.4
N_3	3.3	5	3.2	3.7
H	1.33	1.33	1.33	1.33

Table 7 Bogue's values of OPC used in the research

Oxide	Content (%)	Phase, oxide	Weight (g)
SiO_2	19.51	C3S	61.48
TiO_2	0.39	C2S	11.84
Al_2O_3	3.94	C3A	3.24
Fe_2O_3	4.33	C4AF	13.71
MnO	0.2	O_2	0.35
CaO	58.97	MgO	2.53
MgO	2.43	K_2O	0.23
SO_3^-	5.21	Na_2O	0.65
Cl^-	0.11	SO_3^-	5.42
Na_2O	0.62	MnO	0.21
K_2O	0.22	Cl-	0.11
BaO	0	P_2O_5	0.11
P_2O_5	0.11	ZnO	0.03
ZnO	0.03	Cr_2O_3	0.03
Cr_2O_3	0.03		
CuO	0	Aqueous	41.6

The thermodynamic database is the sole foundation for accurate and complete modeling. GEMS uses cemdata (http://www.empa.ch/cemdata) as the base for solid cementitious substances, including the solubility products of mono-sulfate (C–S–H) phases. During the last decade, the solubility products of more minerals were experimentally determined, turning the thermodynamic database into a more concise and accurate tool (Lothenbach & Zajac, 2019).

4 Results and Discussion

This part presents the results of the physical and mechanical tests of concrete samples for all investigated Control, SCMs, and SWDs mixes. Slump values, absorption ratio at 28 days, and compressive strength at 3 and 28 days are presented in Table 5. Also, the microstructure analysis results considering the percentage of hydrated species and pores percentage at ages 3 and 28 days are presented in the same table. The results of the thermodynamic model for all studied Control and SCMs mixes considering hydration products and phase composition are presented in Table 8. In each of the following sections, the results are analyzed and discussed extensively in light of the experimental results and models carried out in related research works.

4.1 Concrete Results

4.1.1 Workability

Table 5 and Fig. 5 show all concrete mixes' slump values and trends. It can be seen that for BFS mixes, a steady decrease in the value of the slump as the replacement ratio increases were observed for both TW and AW mixes, and the largest value of the decrease reached was 11%, and 18% of the value of the slump of control sample for TW and AW, respectively, at the replacement ratio of 30%. This may be attributed to the agglomeration between particles caused by Van der Waal and electrostatic interaction. The same results were obtained in Anurag et al., 2021. Also, the slump values of AW-BFS mixes increased over TW-BFS mixes by 25%, 23%, 21%, and 15% for Control, 10%, 20%, and 30% cement replacements, respectively. This phenomenon was best explained by Zeta potential measurement. Zeta potential indicates the stability of the formed colloidal solution and the fluid adsorption capability with surfaces in any mix (Jiang et al., 2019). The addition of an alkaline solution containing NaOH increases the pH of the mixed solutions. It hence yields a higher negative zeta potential than the control mix, causing a better particle dispersion and a higher fluidity. The slump results for CKD mixes represent a steady-state behavior reflecting the similarity of chemical behavior and fineness of cement grains. The slump values of AW-CKD mixes increased over TW-CKD mixes by 25%, 19%, 26%, and 26% for Control, 10%, 20%, and 30% cement replacements, respectively.

Table 5 and Fig. 5 show GD and MD slump values. The values indicate that as MD or GD replacement value increases, the workability of concrete mixes decreases.

Table 8 Results from thermodynamic analysis, GEMS

Mix	Item	NaOH molarity				
		0	**0.0043**	**0.02**	**0.2**	**0.313**
OPC	Na/Si	0.06	0.07	0.12	0.65	0.94
	Ca/Si	1.52	1.52	1.49	1.22	1.04
	CH (mass %)	21.3	21.4	21.7	25.0	27.8
	CSH (mass %)	47.3	47.2	47.0	45.0	43.4
	Ettringite (mass %)	19.1	19.0	18.9	19.1	16.9
CKD-20%	Na/Si	0.09	0.10	0.15	0.71	0.96
	Ca/Si	1.49	1.48	1.45	1.14	0.99
	CH (mass %)	25.2	25.3	25.6	29.3	31.5
	CSH (mass %)	43.5	43.4	43.2	41.0	39.5
	Ettringite (mass %)	19.7	19.7	19.6	18.4	13.9
CKD-30%	Na/Si	0.11	0.12	0.17	0.77	0.96
	Ca/Si	1.47	1.46	1.43	1.08	0.96
	CH (mass %)	27.3	27.4	27.8	31.6	33.5
	CSH (mass %)	41.3	41.3	41.1	38.8	37.4
	Ettringite (mass %)	20.1	20.1	20.0	18.9	12.2
BFS-10%	Na/Si	0.06	0.08	0.08	0.65	0.94
	Ca/Si	1.55	1.54	1.54	1.21	1.04
	CH (mass %)	18.7	18.8	18.8	23.4	25.8
	CSH (mass %)	46.9	46.8	46.8	44.0	42.4
	Ettringite (mass %)	18.3	18.3	18.3	17.3	15.0
BFS-20%	Na/Si	0.07	0.08	0.13	0.68	0.94
	Ca/Si	1.58	1.57	1.54	1.20	1.04
	CH (mass %)	16.1	16.2	16.6	21.3	23.8
	CSH (mass %)	46.4	46.3	46.1	43.2	41.4
	Ettringite (mass %)	17.6	17.6	17.5	16.6	13.1
BFS-30%	Na/Si	0.07	0.08	0.13	0.69	0.94
	Ca/Si	1.58	1.57	1.55	1.20	1.04
	CH (mass %)	14.0	14.1	14.5	19.2	21.8
	CSH (mass %)	45.2	45.2	45.0	42.0	40.3
	Ettringite (mass %)	2.3	2.2	16.1	15.2	11.1
LS-10%	Na/Si	0.06	0.08	0.13	0.65	0.94
	Ca/Si	1.55	1.54	1.51	1.22	1.04
	CH (mass %)	24.5	24.6	25.0	28.8	31.2
	CSH (mass %)	45.2	45.1	44.9	42.7	40.9
	Ettringite (mass %)	18.7	18.7	18.6	16.6	14.1
LS-20%	Na/Si	0.07	0.08	0.14	0.60	0.94
	Ca/Si	1.57	1.56	1.53	1.26	1.04
	CH (mass %)	28.5	28.6	28.9	32.4	34.7
	CSH (mass %)	40.8	40.8	40.6	39.8	38.0
	Ettringite (mass %)	14.7	14.7	14.6	12.2	11.5
LS-30%	Na/Si	0.07	0.09	0.15	0.54	0.91
	Ca/Si	1.56	1.55	1.52	1.29	1.05
	CH (mass %)	33.0	33.1	33.4	36.6	38.7
	CSH (mass %)	36.8	36.8	36.6	36.8	35.2
	Ettringite (mass %)	11.7	11.7	11.7	7.5	7.3

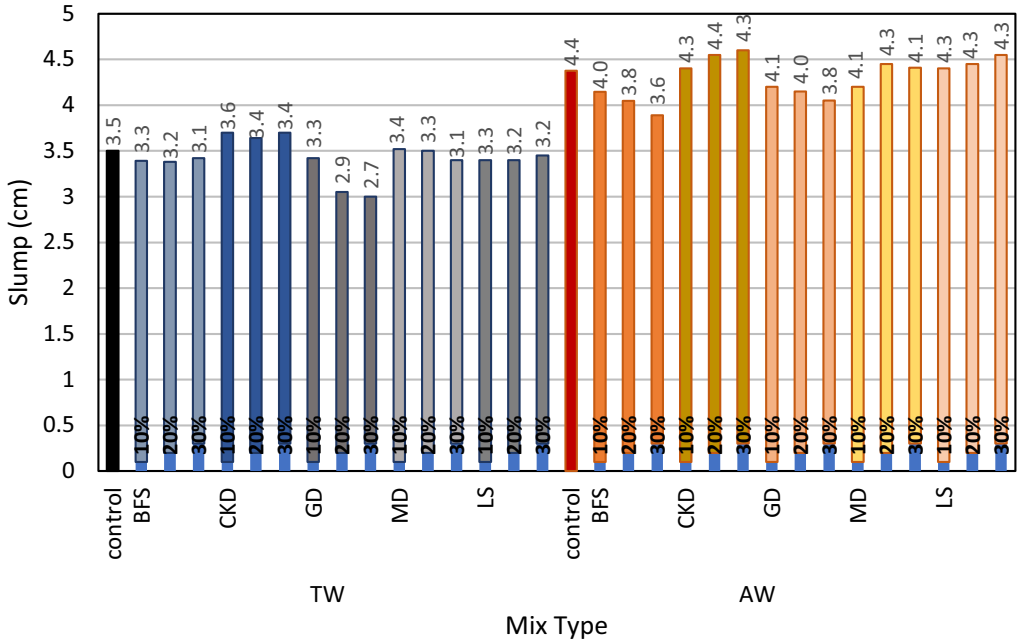

Fig.5 Slump values for all mixes

Considering TW, the largest value of the decrease reached was 23% and 12% of the value of the slump of the control sample for GD and MD, respectively, at the replacement ratio of 30%. As GD or MD acts like a filler with a relatively higher specific surface than ordinary Portland cement, the spaces are filled with GD or MD, leading to more internal friction. In the same context and as was concluded in Ashish (2019), because of the increased fineness of GD and MD, the SWDs powder demands more water content leading to less workable mixes. Considering AW, the largest value of the decrease reached was 14% and 6% of the value of the slump of the control sample for GD and MD, respectively, at the replacement ratio of 30%. As shown in Table 5 and Fig. 5, the slump values of LS mixes decrease incrementally with the increased percentage replacement of cement. The decrease in workability is attributed to the morphological and surface texture effect of LS powder grains since it is of a raw form from the manufacturing process without any further grinding. Morphology and SEM studies (Wang et al., 2018) showed LS powder's rough and porous surface texture, leading to more friction and less workable mixes. The slump values of AW-LS mixes increased over TW-LS mixes by 25%, 30%, 33%, and 35% for Control, 10%, 20%, and 30% cement replacements, respectively.

4.1.2 Physical, Mechanical, and Predictions

4.1.2.1 Water Absorption As seen from Table 5 and Fig. 6a, considering the water absorption values of BFS samples tested at 28 days at the partial replacement of 10%, the water absorption decreased noticeably compared to the control specimens because of the fineness of BFS powder and its pore-filling effect. With the increased amounts of BFS in concrete mixes, the bulk density decreases, and the total porosity increases due to the lower density of BFS. Nevertheless, the low rate of BFS hydration does not provide the hydration products with higher densities (C–S–H) at 28 days but later (El-Didamony et al., 2016). The reduction in the absorption percentage for TW samples was 42.9% for partial replacement of 10%, while, at 20% and 30% BFS replacement, the absorption percentages reached + 3.3% and + 115.4%.

An increase in water absorption refers to increased porosity due to using CKD. Table 5 and Fig. 6b show the absorption percentages values for the CKD concrete samples tested after 28 days. For TW-CKD samples, it can be seen that the absorption percentage increases to 7.7% at a replacement ratio of 10%, then decreases to 5.5% and 8.8% for replacement ratios of 20% and 30%, respectively. This trend was confirmed in Sadek et al. (2017) as a reflection of the considerable amount of free lime, chlorides, and sulfate that exists in the CKD powder

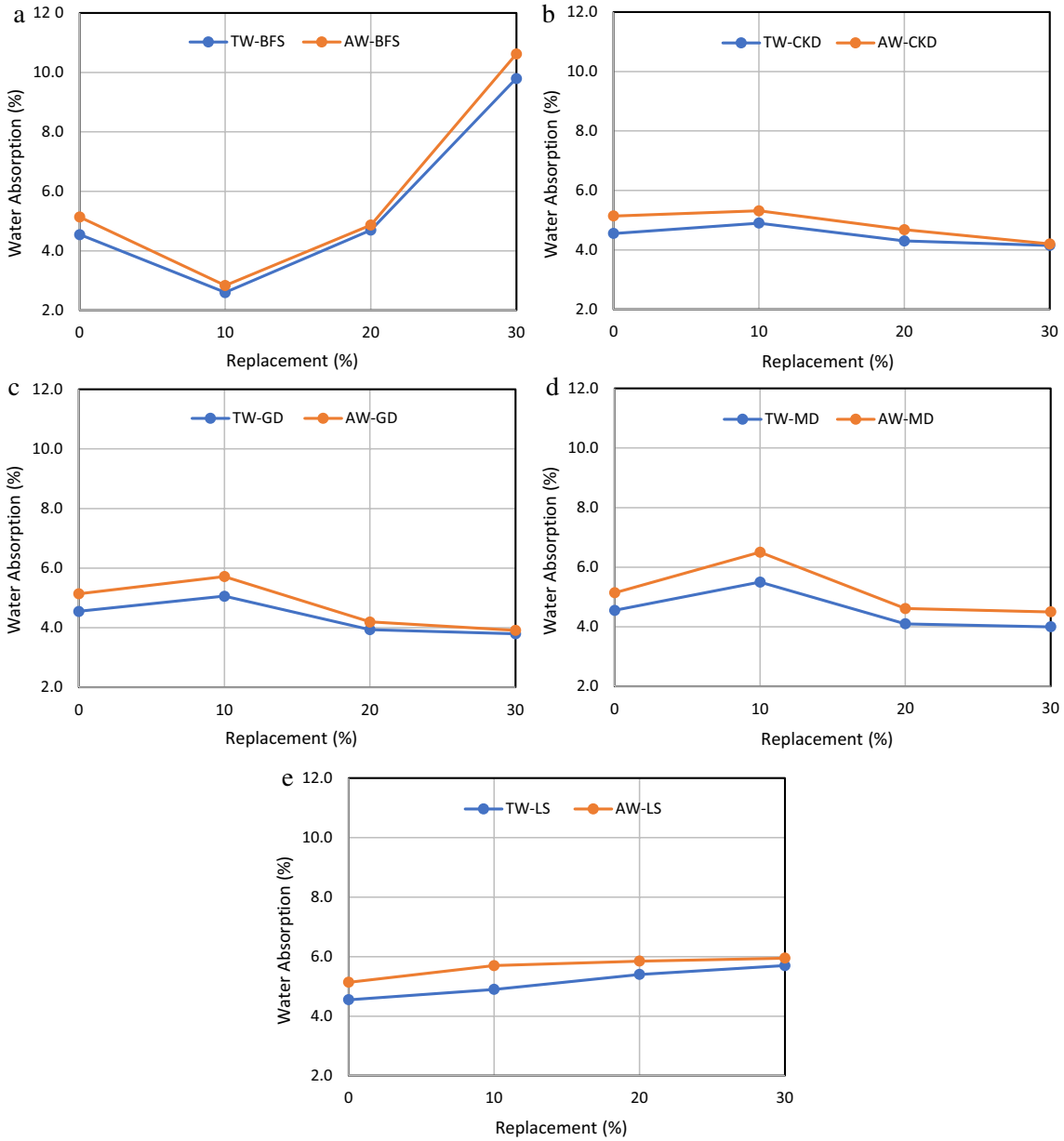

Fig. 6 Water absorption percentages for all mixes: **a** BFS, **b** CKD, **c** GD, **d** MD, and **e** LS samples-age 28 days

leading to the formation of more $Ca(OH)_2$ and the crystallization of hydration products which is followed by the formation of more pores. Considering this explanation, the water absorption was expected to increase further as partial replacement increased, but opposite results were recorded. The activity of CKD is much lesser than the activity of ordinary Portland cement (Mackie et al., 2010), and this leaves more water available for ordinary Portland cement to produce more hydration products (C–S–H) actively and allow for the filling of more pores or at least cutting the continuity of the pores network as observed in Bacarji et al. (2013).

The same trend of CKD samples was observed in GD and MD samples. From Table 5 and Fig. 6c considering TW-GD samples, the absorption percentage increases to 11.2% at a replacement ratio of 10%, then decreases to 13.5% and 16.5% for replacement ratios of 20% and 30%, respectively. Also, from Table 5 and Fig. 6d considering TW-MD samples, the absorption percentage increases to 20.9% at a replacement ratio of 10%, then decreases to

9.9% and 12.1% for replacement ratios of 20% and 30%, respectively. The decrease in water absorption at higher replacement ratios is attributed to the pore-filling resulting from the increased ifneness of GD or MD, providing more nuclei for hydration among aggregate particles and improving fine-particle packing (Galetakis & Soultana, 2016).

As seen from Table 5 and Fig. 6e, with the increase in LS partial replacement, the water absorption of concrete increases as a result of the high specific surface area of the very fine LS powder, which in return demands more water from the mix and hence influences the hydration product and the lubrication around aggregate particles and therefore increase pores (Ergün, 2011). In the same context, a microstructural analysis in Souza et al. (2020) showed that increasing the content of LS is responsible for generating a larger amount of pores with a smaller diameter allowing interconnection between the pores and hence increasing the water absorption. Considering TW samples, the absorption percentage increases to 7.7%, 18.9%, and 25.3% at a replacement ratio of 10%, 20%, and 30%, respectively.

On the other hand, when comparing the AW results to the TW results, it can be seen that an overall increase in the absorption percentages values was achieved following the same systematic behavior considering all materials. The percentage increase in absorption percentages of AW-control samples compared to TW-controls was 13%. In the same context, it was found in Berodier, 2015 that at 7 and 28 days, the porosity in samples made with AW containing NaOH was 10% higher than control samples made with TW and that the capillary porosity had increased with a slightly fewer radius more than the ones of control samples. It is worth mentioning that the addition of NaOH increases the pH of the pore solution in samples, which increases the solubility of ettringite.

In Chamrova (2010), it was proven that Young's modulus of CSH is 22.6 GPa, while it is 22.4 GPa for ettringite, which means they both influence the mechanical properties. With lower amounts of ettringite, higher capillary pores are created.

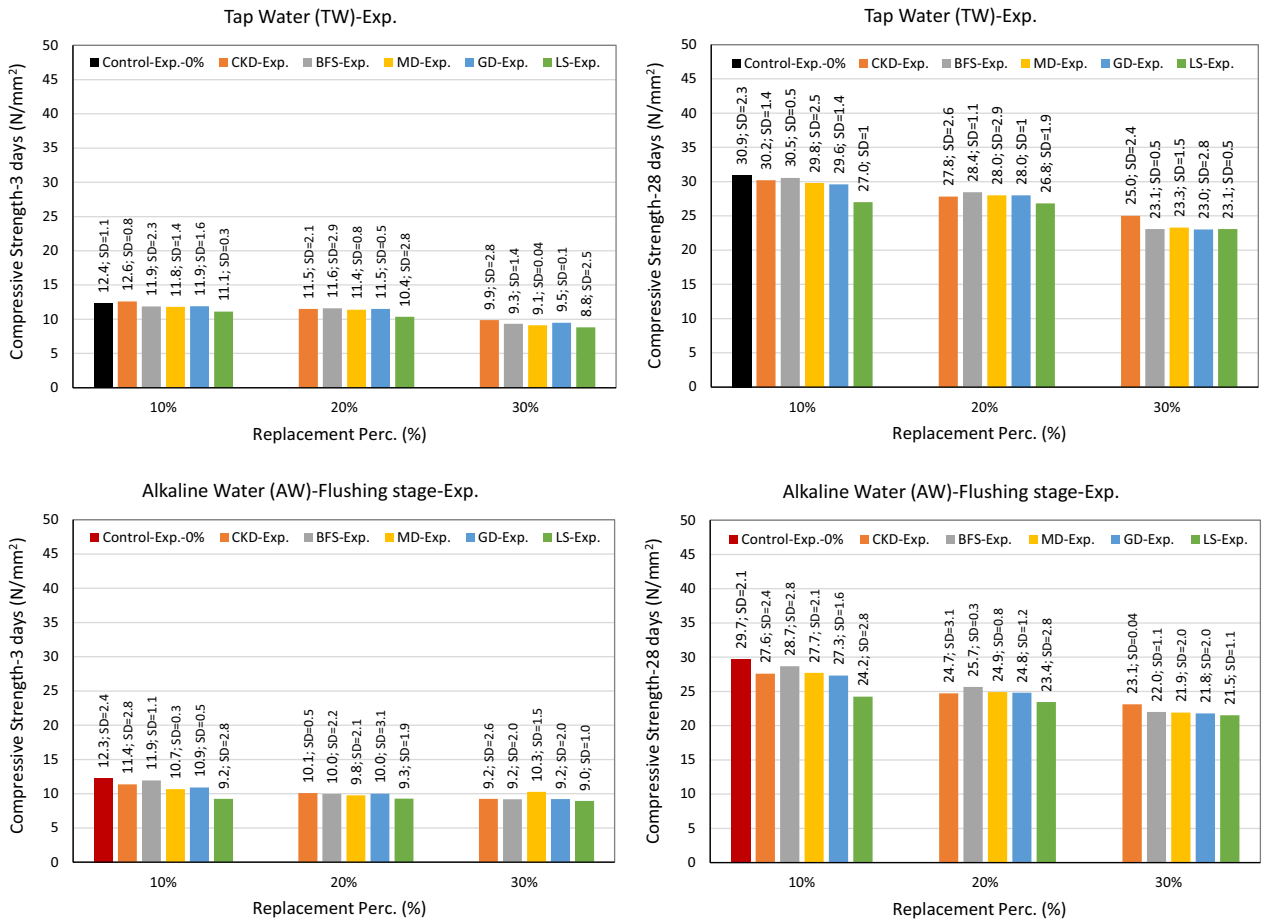

Fig. 7 Compressive strength results for TW and AW mixes at 3 and 28 days

4.1.2.2 Compressive Strength Table 5 and Fig. 7 show the compressive strength results of different concrete mixes at 3 and 28 days, respectively, considering mixes of TW and AW. As seen in Table 5 and Fig. 7, considering the mixes with tap water (TW), at the age of 28 days, the control mix gave a compressive strength of 31 N/mm^2. The values closest to the control result were those materials mixed with 10% cement replacements by weight, where the compressive strength result of all materials approached the control result except for limestone, which had the lowest percentage decrease by 13%. The compressive strength of the samples was reduced by 2%, 1%, 4%, and 4% for CD, BFS, MD, and GD, respectively. The BFS samples showed superiority over the rest of the SCMs or SWDs samples, which is attributed to the relatively active chemical components in BFS, especially SiO_2, and CaO, which are responsible for activating pozzolanic activity (Roslan et al., 2016). Also, it is expected at later ages, after 28 days, that the BSF reacts with CH to perform a pozzolanic effect and further improve the strength (Wu et al., 2021). Considering the mixes made with 20% SCMs or SWDs cement partial replacements, it can be seen that all materials had a lower compressive strength value than the Control and those samples of 10% partial replacements. The compressive strengths of the 20% samples were reduced by 10%, 8%, 10%, 10%, and 13% for CD, BFS, MD, GD, and LS, respectively. The water demand of LS affected both workability and compressive strength by decreasing hydration products. The increased water demand of LS contributed to creating an increased porosity and hence affecting the compressive strength, Fig. 6e, (Souza et al., 2020).

Considering the mixes made with 30% SCMs or SWDs cement partial replacements, it can be seen that all materials had the lowest compressive strength values among all replacement ratios. The compressive strength of the samples was reduced by 19%, 25%, 25%, 26%, and 25% for CD, BFS, MD, GD, and LS, respectively. The relative superiority of CD strength values in the 30% replacement samples is due to its enhanced hydration products due to the relatively active silica and calcium oxide and the improvement in the concrete microstructure (Alnahhal et al., 2018). As seen from the results for all partial replacement ratios, the decrease in compressive strengths of GD and MD samples is attributed to the crystalline structure of both GD and MD powders. The partial replacement is considered as replacing reactive cementitious material (OPC) with a non-reactive material (GD and MD), and the effect of those replacement powders was limited to the filler effect, which is dominated by the particle packing with a negligible contribution to CSH and hence to strength (Bacarji et al., 2013). As seen in Table 5 and Fig. 7, considering the mixes with alkaline water (AW), at 28 days, the control mix gave a compressive strength of 29.7 MPa. The values closest to the control result were those materials mixed with 10% cement replacements by weight, and the same trend as those of TW-10% was observed in AW-10% samples. The compressive strength of the samples at 10% replacement was − 7%, − 3%, − 7%, − 8%, and − 18% for CD, BFS, MD, GD, and LS, respectively. Considering the mixes made with 20% AW-SCMs or AW-SWDs cement partial replacements, it can be seen that all materials had a lower compressive strength value than the Control and those of 10%. The compressive strength of the samples at 20% replacement was − 17%, − 14%, − 16%, − 16%, and − 21% for CD, BFS, MD, GD, and LS, respectively. Considering the mixes made with 30% AW-SCMs or AW-SWDs cement partial replacements, it can be seen that all materials had the lowest compressive strength values among all replacement ratios. The compressive strength values of the samples were reduced by 22%, 20%, 21%, 21%, and 23% for CD, BFS, MD, GD, and LS, respectively.

Compared to the samples of TW, the compressive strength results of TW samples were generally lesser, and the AW-control was − 4% compared to TW. Considering 10% replacement, the results of AW samples were − 9%, − 6%, − 7%, − 8%, and − 10% compared to TW samples for CD, BFS, MD, GD, and LS, respectively. For 20% replacement, the results of AW samples were − 11%, − 10%, − 11%, − 11%, and − 13% compared to TW samples for CD, BFS, MD, GD, and LS, respectively. Finally, for 30% replacement, the results of AW samples were − 8%, − 5%, − 6%, − 5%, and − 7% compared to TW samples for CD, BFS, MD, GD, and LS, respectively. Among AW samples, it can be seen that the only samples that survived the negative impact of AW on compressive strength were AW-BFS-30% and AW-MD-30%. The early compressive strength results (3 days) considering TW or AW for all SCMs or SWDs samples were close to the overall trend.

Tests done at 28 days provide a good indication of the strength of the concrete. In some cases, after the mixtures, there is expected to be a noticeable improvement in the mechanical properties (compressive strength) for the older ages (90 days) due to the delayed reaction of materials such as BFS. In future work, it will be conducted to explore this phenomenon further.

As can be seen from the individual results of AW samples and their comparative ratios with similar compositions in TW mixes, an overall similarity in the trends considering 10%, 20%, and 30% partial replacements

samples but with an overall decrease in the compressive strength values as a direct impact of AW was recorded. It was found in Berodier, 2015 that the degree of reaction in tri calcium silicate (C_3S) for samples made with TW is increasing continuously until it is almost consumed at the age of 28 days. The same case was observed for the degree of hydration of tri calcium aluminate (C_3A). But on the other hand, the samples made with NaOH as an alkaline solution (AW) showed 10% less hydration considering C_3S and 20% less hydration of C_3A. This phenomenon was further investigated from two perspectives. The first one relates to relative humidity (RH), where the measurements showed a constant complete (100%) RH for up to 28 days for samples made with TW. Considering the samples with AW, the measurements showed a continuous decrease in RH for up to 7 days until it reaches about 90% and then stabilizes after that, which refers to lower water activity due to the higher concentrations of ions in the pore solution considering the AW samples. The second perspective for the decrease in the degree of hydration in the AW samples is based on the change in the aluminate ions concentration (which increases dramatically) as a direct result of the increased solubility of aluminate from cement, which inhibits the silica dissolution (Quennoz & Scrivener, 2013). Another comprehensive explanation for this effect of AW on the mechanical properties of concrete with different replacement ratios of SCMs and SWDs materials under normal mixing and curing conditions needs further microstructure analysis and thermodynamics modeling through the following sections. Despite a relatively minor decline in the compressive strength of concrete samples for certain replacement materials and ratios, this decrease remains within the safe and acceptable parameters dictated by design and code requirements for reinforced concrete and plain concrete components. This is consistent with what was recently found in a review article (Gudainiyan & Kishore, 2023).

4.2 Microstructure Results

The image analysis of the backscattered electron SEM images (BSE) of the different SCMs and SWDs samples made during the experimental work at 3 and 28 days, respectively, can quantify many aspects of microstructural development and microstructure components (Bailey & Chescoe, 1979). Examples of the extracts of the BSE images are the remaining anhydrous materials that can be identified, the quantities and distribution of CH, and the amount and size distribution of porosity in the cement pastes. The analysis of BSE images taken at later ages, considering the number of pores and their distribution, the amounts of hydrates, and the amount of CH, may indicate the expected mechanical performance for concrete made of these pastes. Fig 8 shows the backscattered electron images of Control-TW-3 days specimens. At 350× magnification, the BSE image shows cement grains with calcium silicate hydrate (CSH) shells. This can be observed more clearly at a 2000× magnification, where the image also reveals needle-like shapes (representing ettringite), pores, and widespread CSH clouds. These features indicate that the specimen has undergone a hydration reaction, which is expected to occur when cement is mixed with water. The presence of ettringite and the CSH clouds indicate that the hydration reaction has proceeded to a more advanced state, with the cement grains becoming enveloped in calcium silicate hydrate. The pores observed in the image are likely caused by the expansion of the cement grains due to the hydration reaction.

Fig. 9 shows the backscattered electron images of the Control-AW-3 days sample at 350× and 2000× magnifications. At 350× magnification, the pores are relatively wide and randomly distributed. At 2000× magnification, a larger area of pores, CH plate formations, CSH clouds, and Ettringite needles can be seen. The inverted copy of the 2000× magnification image further reveals the fine details of these features. This indicates that the sample has a high porosity and a wide variety of crystalline

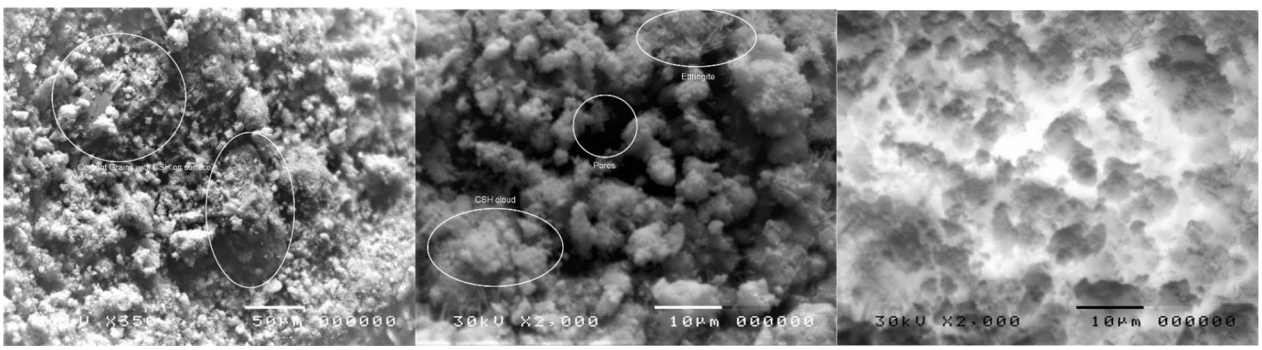

Fig. 8 BSE images of Control-TW-3 days specimens

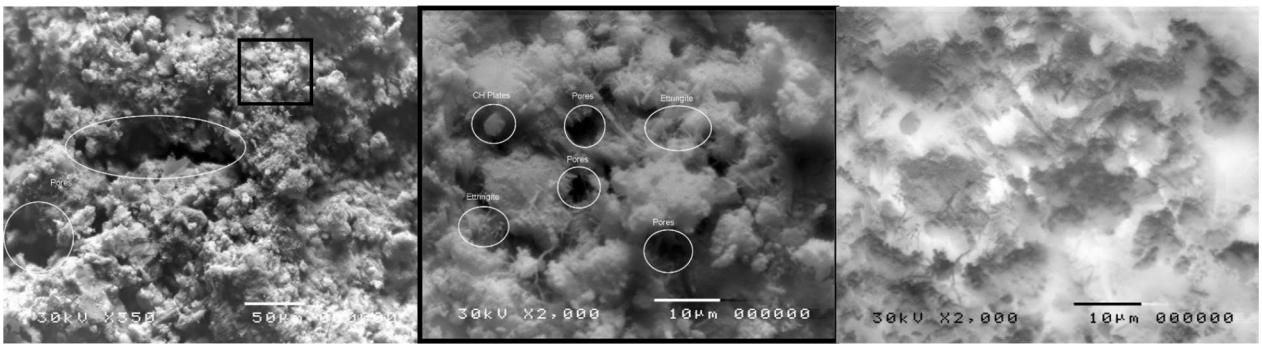

Fig. 9 BSE images of Control-AW-3 days specimens

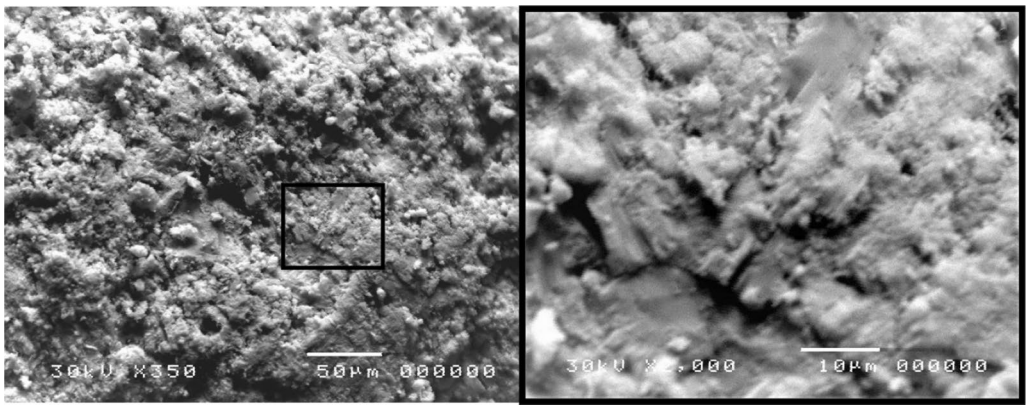

Fig. 10 BSE images of Control-TW-28 days specimens

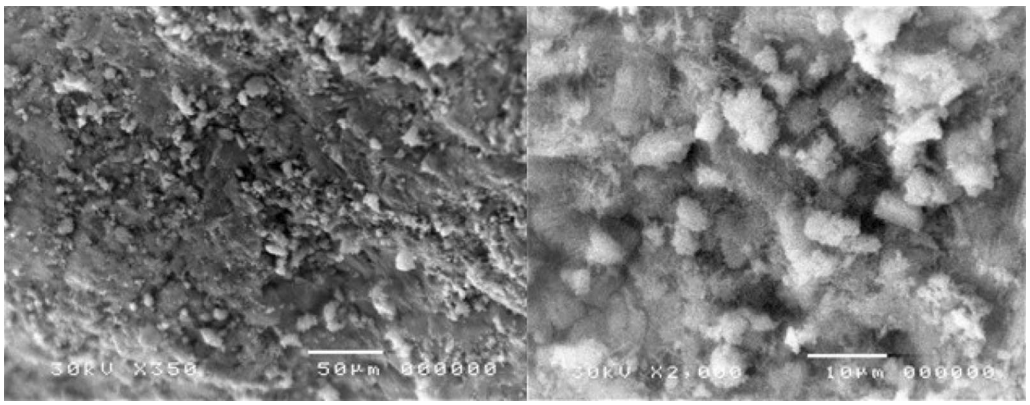

Fig. 11 BSE images of Control-AW-28 days specimens

structures. Fig. 10 shows Control-TW-28 days BSE photos. It can be seen from the 350× Magn. photo a homogeneous microstructure with almost negligible pores referring to almost complete hydration, and this solid and flawless structure is realized from its 2000× Magn. part photo.

Fig. 11 shows Control-AW-28 days BSE photos. It can be seen from the 350× Magn. photo, a homogeneous microstructure with almost negligible pores referring to almost complete hydration but with less CSH, while large amounts of Ettringite needles are noticed in the 2000× Magn. photo.

When comparing BSE photos from 3 and 28 days, it can be seen that the hydration process has caused the development of hydration products, such as calcium silicate hydrate (C–S–H) and calcium hydroxide (CH). These hydration products help to fill in the pores in the microstructure of the samples, thus decreasing the porosity and densifying the material. This process of densification is an important part of the hydration process and the resulting microstructure of the sample. Fig 12 shows BFS-20%-TW-3 days BSE photos. The BSE-Magn.350× for samples at the age of 3 days shows ordinary Portland cement-hydration products, while a Magn.2000× photo and its inverted copy for a part of the photo show BFS grains that actively worked as a nucleation site for hydration and the BFS itself are expected to actively perform a complete hydration product at ages beyond 28 days; also

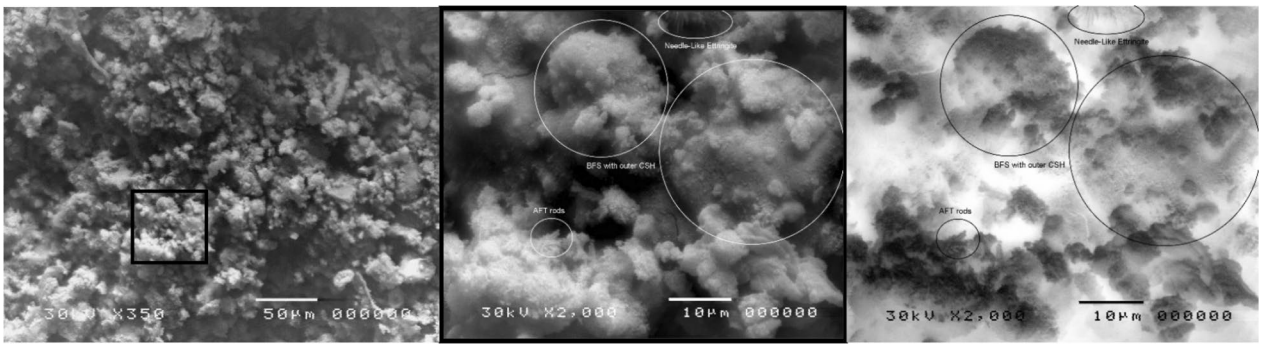

Fig. 12 BSE images of BFS-TW-3 days

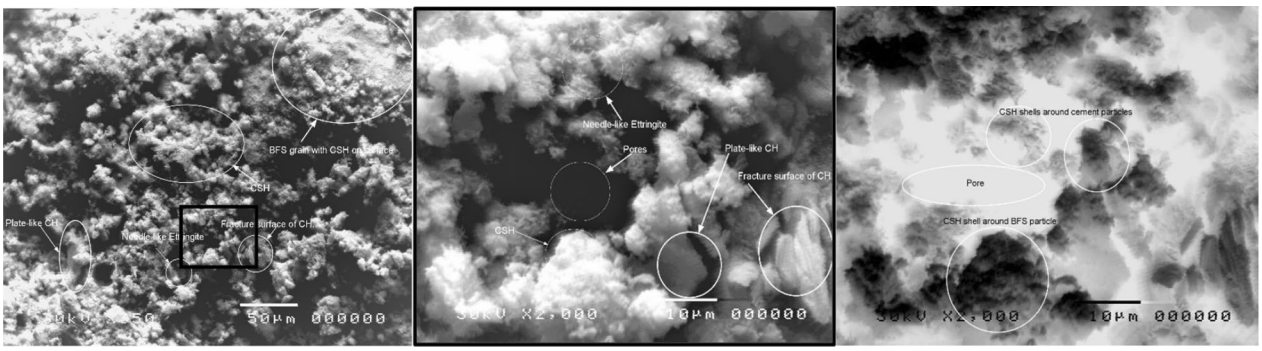

Fig. 13 BSE images of BFS-AW-3 days

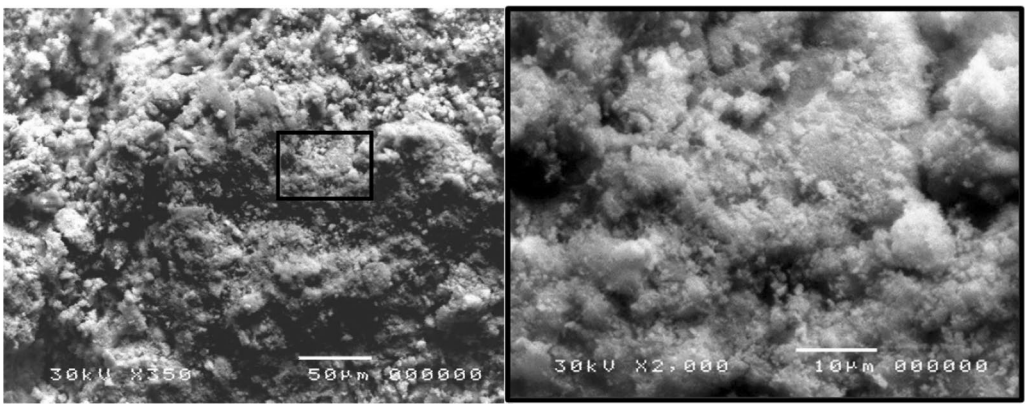

Fig. 14 BSE images of BFS-TW-28 days

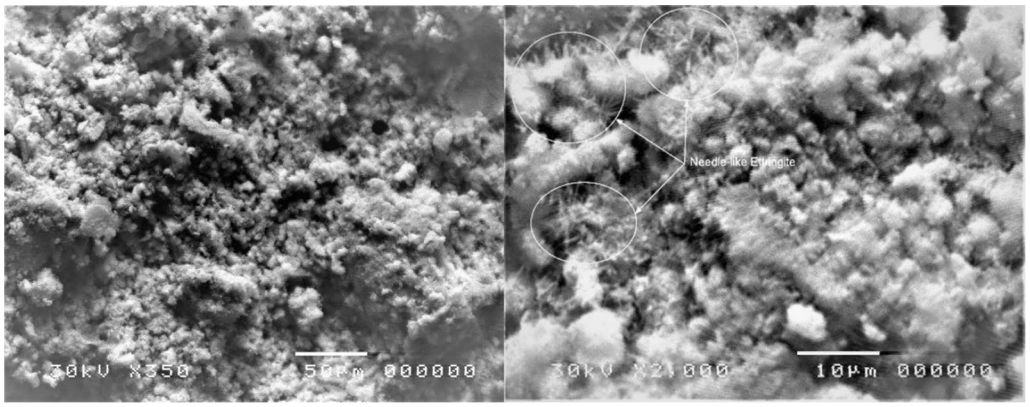

Fig. 15 BSE images of BFS-TW-28

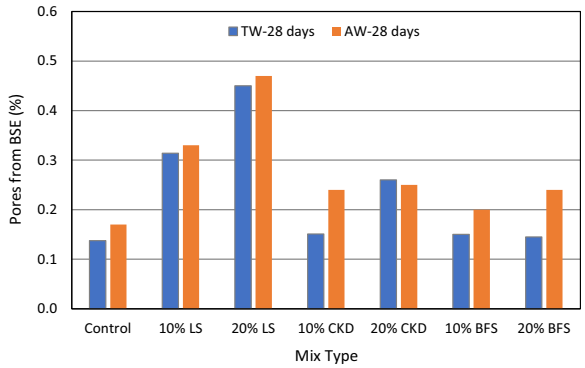

Fig. 16 Pores from the histogram analysis of BSE at 28 days

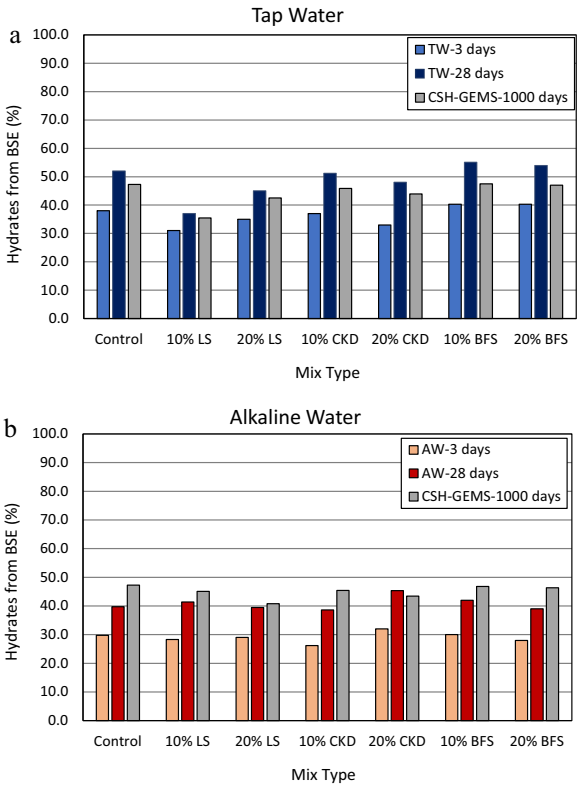

Fig. 17 Hydrates percentage from the histogram analysis of BSE at 28 days and thermodynamic modeling (GEMS); **a** TW, **b** AW

clouds of CSH, AFT rods, and needle-like ettringite are shown.

Fig. 13 shows BFS-20%-AW-3 days BSE photos. The BSE-Magn.350× for samples at the age of 3 days shows an increased pore formation, CSH around BFS grains, plate-like CH, and needles-like ettringite. A 2000× Magn. part and its inverted copy photos show the increased amounts of ettringite, CSH, CH, and the continuous pores closely. In general, CH plates are considered a weak structure inside cement paste. Thus, the existence of SCMs favors the consumption of more CH into CSH.

Fig. 14 shows the BSE photos of BFS-20%-TW-28 days, which is a type of blended cement with 20% Blast Furnace Slag (BFS) content and 28 days of curing time. The BSE-Magn. 350× and Magn. 2000× photos at 28 days show a significant increase in hydration products compared to the 3-day samples, which have minimal pores and a solid microstructure. Fig. 15 shows the BSE photos of BFS-20%-AW-28 days, which also has 20% BFS content but with 28 days of curing time in an air-cured environment. The BSE-Magn. 350× photo at 28 days shows an increase in pores compared to the TW samples, while the Magn. 2000× photo shows an increase in needles-like Ettringite, which indicates a more advanced hydration process. The increased amount of Ettringite suggests a higher rate of hydration and improved cementitious properties.

Table 5 and Fig. 16 show the pores percentage at 28 days taken from the histogram at a certain threshold that describes the pores for each BSE image. It can be seen that the control mix gave the least pores while LS samples had the highest pores values. For

TW results, the percentage increases in pores compared to the control mix were 121%, 221%, 7%, 86%, 7%, and 0% for mixes 10%LS, 20%LS, 10%CD, 20%CD, 10%BFS, and 20%BFS, respectively. For AW results, the percentage increases in pores compared to the control mix were 94%, 176%, 41%, 47%, 18%, and 41% for mixes 10%LS, 20%LS, 10%CD, 20%CD, 10%BFS, and 20%BFS, respectively. For accuracy and a good representation of the sample's size (Scrivener, 2004), all the values were taken from the 350 magnification BSE. As explained in sec. 4.1.2.1 and sec. 4.1.2.2., these results are in good agreement with water absorption results, where NaOH solution had proved a negative effect on the porosity of cement pastes and an inverse relation between porosity and mechanical strength are greatly expected.

It can be seen that the alkaline solution harmed the CSH and other hydration products as a direct result of the increase in ion concentration and the decrease in the relative humidity during the hydration process. From Fig. 17, considering the results from thermodynamic modeling and for the hydrates of TW samples from BSE image processing and compared to the control mix, the ratios were 0.75, 0.90, 0.97, 0.93, 1.00, and 0.99 for mixes 10%LS, 20%LS, 10%CD, 20%CD, 10%BFS, and 20%BFS, respectively. For the hydrates of AW samples from BSE image processing and compared to the control mix, the ratios were 0.95, 0.86, 0.96, 0.92, 0.99, and 0.98 for mixes 10%LS, 20%LS, 10%CD, 20%CD, 10%BFS, and 20%BFS, respectively. The ratios of TW hydrates to AW hydrates were 0.999, 1.273, 0.960, 0.990, 0.988, 0.987, and 0.986 for Control, 10%LS, 20%LS, 10%CD, 20%CD, 10%BFS, and 20%BFS, respectively. The results of the GEMS show that the effect of the alkaline solution on the hydration products is much less than in the case of hydrates from BSE image analysis. To the authors' knowledge, there is no clear explanation for these minor differences. However, more advanced techniques in the chemical analysis of the samples can be used to make more accurate inputs to the thermodynamic modeling software.

4.3 Thermodynamic Results

The principles of thermodynamics are based on the principles of mass equilibrium, where the compositions of the starting materials are used to derive the stable phase assemblage. In this research work, the starting materials in the thermodynamic model (GEMS) have been used differently in its activity and reaction rate. Whether the almost fully activated material (cement) or the supplementary cementitious materials, whose activity has been limited to no more than approximately 50%, are defined in the input stage. The solubility products for cement minerals, including CSH, ettringite, hydrogarnet, and hydrotalcite, were taken from the Cemdata14. Upon decalcification, CSH shows incongruent solubility behavior where dissolved Ca and Si concentrations vary with Ca/Si ratio and pH degree (Lothenbach et al., 2011). Ca/Si ratio controls the end members of the CSH system, whether jennite $(CaO)_{1.67}(SiO_2)_1{\cdot}(H_2O)_{2.1}$ or tobermorite $(CaO)_{0.83}$ $(SiO_2)_1{\cdot}(H_2O)_{1.3}$. Table 8 and Fig. 18 show the Ca/Si and Na/Si ratios versus NaOH molarity. The Ca, Na, and Si values are computed from CSH components resulting from GEMS output analysis. It is shown that as Na concentration increases, the Ca/Si ratio decreases. The increase in Na/Si is steep, and accordingly, the Ca/S decreases steeply after a molarity of 0.02 (800 ppm). The analysis of CD-10% mixes has been stopped due to convergence problems. When comparing the Ca/Si ratios of all mixes with the ordinary Portland cement mix, the relative ratios are 0.98, 0.97, 1.02, 1.04, 1.04, 1.02, 1.03, and 1.03 for CD20%, CD30%, BFS10%, BFS20%, BFS30%, LS10%, LS20%, and LS30%, respectively. For ordinary Portland cement, the relative ratios between Ca/Si ratio for NaOH different molarities and the TW mix are 1.00, 0.98, 0.80, and 0.68 for NaOH molarity of 0, 0.0043(173 ppm), 0.02(800 ppm), 0.2(8000 ppm), and 0.313(12,500 ppm). For ordinary Portland cement, the relative ratios between Ca/Si ratio for NaOH different molarities and the TW mix are 1.00, 0.98, 0.80, and 0.68 for NaOH molarity of 0, 0.0043(173 ppm), 0.02(800 ppm), 0.2(8000 ppm), and 0.313(12,500 ppm). The rest of the mixes have almost the same figures, and as mentioned earlier, a stable Ca/Si value is noticed for 0.0043 and 0.02 mol, then a sudden decrease is noticed at 0.2 and 0.313 mol. The pH of the pore solution is increased by alkali salts lowering the calcium and increasing the concentration of the dissolved silicon leading to an overall decrease in the Ca/Si ratio (Lothenbach & Nonat, 2015). This leads to a change in the structure of the gel, and hence at later ages, this will affect the mechanical properties.

Table 8 and Fig. 19 show the CSH values as mass % from GEMS. When comparing CSH values of all mixes with the ordinary Portland cement mix, the relative ratios are 0.92, 0.87, 0.99, 0.98, 0.96, 0.96, 0.86, and 0.78 for CD20%, CD30%, BFS10%, BFS20%, BFS30%, LS10%, LS20%, and LS30%, respectively. These values show that BFS10% and BFS20% were the optimum mixes considering the CSH percentages, while CD30%, LS20%, and LS30% had the lowest CSH values among all mixes. Also, the values of CSH decreased with the increase in molarity, and while the CSH values for all mixes were stable until 0.02 mol, they began to decrease sharply. For ordinary Portland cement, the relative ratios between CSH for NaOH different molarities and the TW mix are 1.00, 0.99, 0.95, and 0.92 for NaOH molarity of 0, 0.0043(173 ppm), 0.02(800 ppm), 0.2(8000 ppm), and 0.313(12,500 ppm).

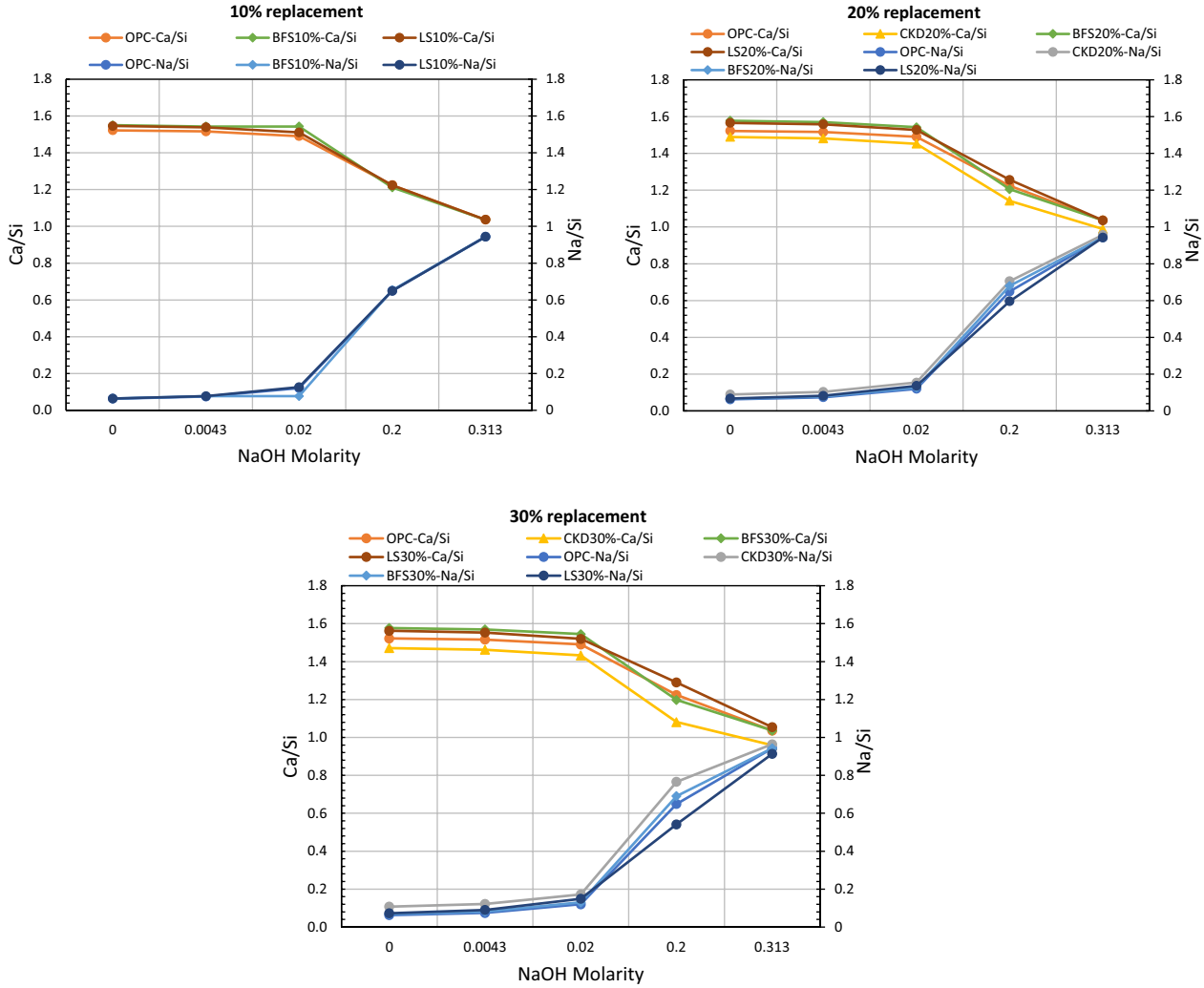

Fig. 18 Ca/Si and Na/Si ratios versus NaOH molarity for all mixes from GEMS analysis

CSH represents the main hydrated components responsible for mechanical performance and ettringite, which has a similar modulus of elasticity. The effect of alkalis on the mechanical strength, among other characteristics of cement mortars, was studied in Shayan and Ivanusec (1989). It was found that an increasing addition of NaOH from 0.5 mol to 4.5 mol gradually lowered the strength of cement mortars at early and later ages as well. Table 8 and Fig. 18 show an inverse relation between CSH and CH for each mix. An increase follows the decrease in CSH in CH for any mix. When comparing CH values of all mixes with ordinary Portland cement mix, the relative ratios are 1.18, 1.28, 0.88, 0.76, 0.66, 1.15, 1.34, and 1.55 for CD20%, CD30%, BFS10%, BFS20%, BFS30%, LS10%, LS20%, and LS30%, respectively. For all mixes, the CH increases with the increase in NaOH molarity, and the highest increases were noticed at mixes BFS30%, BFS20%, and BFS10%, respectively, at a NaOH molarity of 0.313. The lowest increases in CH were noticed in LS30%, LS20%, and CD30% mixes, respectively.

In Way and Shayan, (1989), an increase in the rate of formation of CH in ordinary Portland cement with the increasing concentration of NaOH in the mixing water was noted. Also, alkalis in cement paste promote CH nucleation with a hexagonal platelet morphology (Gallucci & Scrivener, 2007).

Table 8 and Fig. 20 show the ettringite values as mass % from GEMS for all mixes. When comparing ettringite values of all mixes with ordinary Portland cement mix, the relative ratios are 1.03, 1.06, 0.96, 0.92, 0.12, 0.98, 0.77, and 0.62 for CD20%, CD30%, BFS10%, BFS20%, BFS30%, LS10%, LS20%, and LS30%, respectively. For all mixes, the ettringite values decrease with the increase in NaOH molarity, and the highest increases were noticed at mixes BFS30%, BFS20%, and BFS10%, respectively, at NaOH molarity of 0.313. The lowest increases in CH were

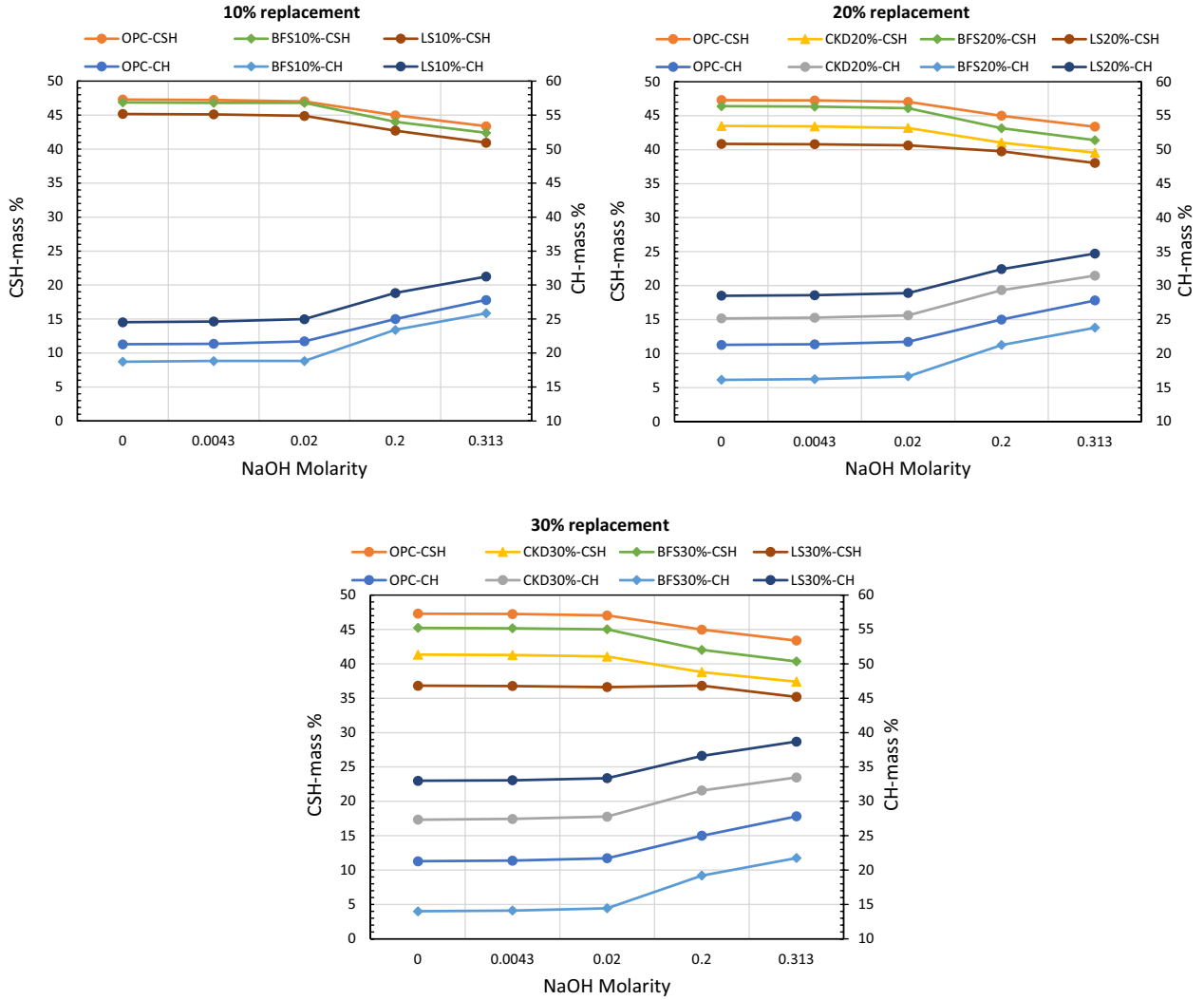

Fig. 19 CSH and CH mass percentages versus NaOH molarity for all mixes from GEMS

noticed in LS30%, LS20%, and CD30% mixes, respectively. These results match the observations of Bizzozero et al. (2014), where the addition of NaOH increased the pH of the pore solution leading to an increase in the solubility of ettringite.

5 Conclusion

Recycling cementitious materials, stone dust, and alkaline water in concrete manufacturing has a significant potential to reduce the environmental impact of the industry and make concrete production more sustainable. Recycling these materials can reduce the number of natural resources needed and the amount of waste generated and reduce energy consumption and carbon dioxide emissions. However, several barriers to implementing waste recycling in concrete production exist, such as technological limitations, difficulties in changing existing production processes, and the lack of financial incentives. More research is needed to understand the benefits, potential costs and risks, and technical and economic implications of increasing the adoption of recycling in concrete production. In this study, the utilization of alkaline solution containing NaOH from a pots factory, SCMs, and SWDs from cement, steel, and ornamental factories in an industrial city in Egypt has been extensively studied in the manufacturing of normal concrete under normal casting and curing conditions. To study the effects of these materials on concrete, physical, mechanical, microstructure, and thermodynamic modeling were used to assess the suitable partial replacement ratios of powders and the effect of the alkaline solutions. The following was concluded:

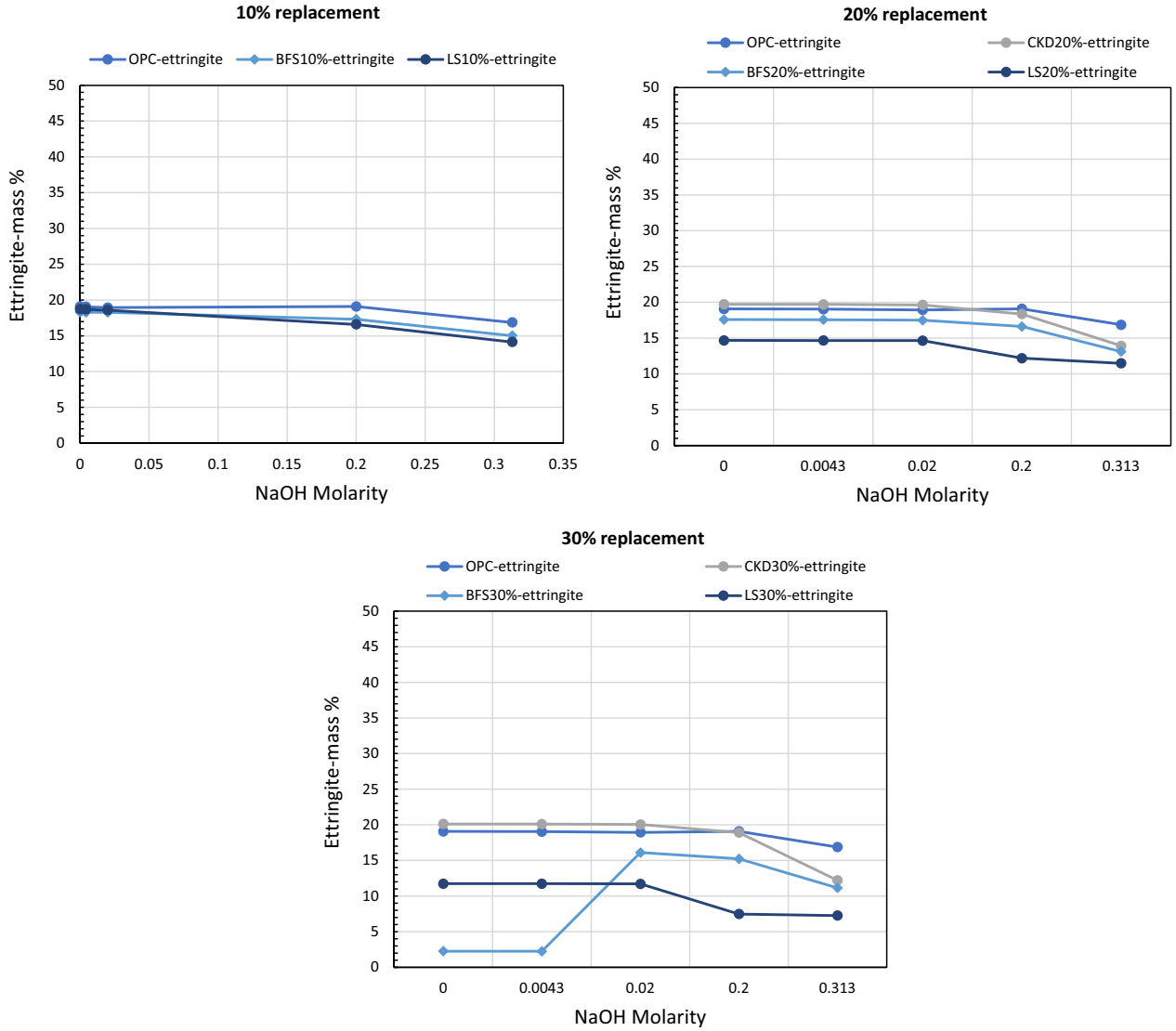

Fig. 20 Ettringite mass percentages versus NaOH molarity for all mixes from GEMS analysis

- The use of alkaline water (AW) led to a percentage increase in a slump of 26% compared to mixing with tap water (TW) as a reflection of the zeta potential effect.
- The measured water absorption percentages for samples made of AW were higher than those of TW as NaOH increases the pH of the pore solution in samples, increasing the solubility of ettringite and increasing pore percentages.
- Most of the TW and AW samples with SCMs or SWDs powders had a compressive strength close to the corresponding control mix at a cement replacement ratio of 10% with an advantage of the SCMs due to their pozzolanic effect. Meanwhile, NaOH in the AW affected the hydration of C3S and C3A, leading to a decrease in the compressive strength of AW samples compared to TW samples.
- The presence of SCMs powders at the replacements percentages of 10 and 20% gave the most similar microstructure to control mixes considering pores and percentages of hydrates species.
- As observed from the microstructure analysis, AW slightly increased the pores and decreased the percentages of hydrates species.
- Thermodynamic analysis showed a steep decrease in Ca/Si ratios and a steep increase in Na/Si ratios for samples made with the pots' factory-flushed NaOH solution after a molarity of 0.02.

- Thermodynamic analysis showed a steep decrease in CSH mass percentage and a steep increase in CH mass percentage for samples made with the pots' factory-flushed NaOH solution after molarity of 0.02.
- Thermodynamic analysis showed a decreased ettringite mass percentage with increased NaOH molarity.

Acknowledgements
The first and second authors would like to acknowledge the chairman of Nouval company Magdi M. Afifi, the head of the quality sector, Alhussain M. Abushady, and the IT manager, Ahmed. M. Elshoweikh for providing alkaline water to accomplish the experimental work of this research.

Author contributions
SHAT: conceptualization, investigation, methodology, visualization, validation, writing—original draft. SEZ: investigation, methodology, validation, visualization, writing—original draft. RAES: investigation, methodology, visualization, writing—original draft. HEM: visualization, validation, writing—review and editing. All authors read and approved the final manuscript.

Authors' information
Sherif H. Al-Tersawy is an Associate Professor and Chairman of the Civil Engineering Department, Higher Technological Institute (HTI), 10th of Ramadan City, 44,629, Egypt.
Sahar E. Zakey is an Assistant Professor of the Civil Engineering Department, Higher Technological Institute (HTI), 10th of Ramadan City, 44,629, Egypt.
Rasha A. El-Sadany is an Assistant Professor Radiation Engineering Department at National Center for Radiation Research and Technology, Egyptian Atomic Energy Authority, Cairo, 11,787, Egypt.
Hossam El-Din M. Sallam is a Professor of the Materials Engineering Department, Faculty of Engineering, Zagazig University Zagazig 44,519, Egypt.

Funding
Open access funding provided by The Science, Technology & Innovation Funding Authority (STDF) in cooperation with The Egyptian Knowledge Bank (EKB).

Availability of data and materials
All data generated or analyzed during this study are included in this published article.

Declarations

Informed consent
Informed consent was obtained from all individual participants included in this study.

Competing interests
The authors declare that they have no competing interests.

Received: 30 December 2022 Accepted: 16 April 2023
Published online: 14 August 2023

References

Abdel-Gawwad, H. A., Heikal, M., Mohammed, M. S., El-Aleem, S. A., Hassan, H. S., García, S. R. V., et al. (2019). Sustainable disposal of cement kiln dust in the production of cementitious materials. *Journal of Cleaner Production, 20*(232), 1218–1229.
Abukersh, S. A., & Fairfield, C. A. (2011). Recycled aggregate concrete produced with red granite dust as a partial cement replacement. *Construction and Building Materials, 25*(10), 4088–4094.
Abzaev, Y., Gnyrya, A., Korobkov, S., Gauss, K., Boyarintsev, A., & Tomrachev, S. (2019). Thermodynamic modeling of Portland cement without mineral additives. *Journal of Physics: Conference Series.* https://doi.org/10.1088/1742-6596/1145/1/012016
Alnahhal, W., Taha, R., Al-Nasseri, H., & Nishad, S. (2018). Effect of using cement kiln dust as a nano-material on the strength of cement mortars. *KSCE Journal of Civil Engineering, 22*(4), 1361–1368.
Al-Tersawy, S. H., El-Sadany, R. A., & Sallam, H. E. M. (2021a). Long-term behavior of normal weight concrete containing hybrid nanoparticles subjected to gamma radiation. *Archives of Civil and Mechanical Engineering, 21*(1), 1–18.
Al-Tersawy, S. H., El-Sadany, R. A., & Sallam, H. E. (2021b). Experimental gamma-ray attenuation and theoretical optimization of barite concrete mixtures with nanomaterials against neutrons and gamma rays. *Construction and Building Materials, 289*, 123190. https://doi.org/10.1016/j.conbuildmat.2021.123190
Arel, H. Ş, & Shaikh, F. U. A. (2019). Semi-green cementitious materials from waste granite by considering the environmental, economic, and health impacts: A review. *Structural Concrete, 20*(1), 455–470.
Ashish, D. K. (2019). Concrete made with waste marble powder and supplementary cementitious material for sustainable development. *Journal of Cleaner Production, 20*(211), 716–729.
Bacarji, E., Toledo Filho, R. D., Koenders, E. A. B., Figueiredo, E. P., & Lopes, J. L. M. P. (2013). Sustainability perspective of marble and granite residues as concrete fillers. *Construction and Building Materials, 45*, 1–10.
Bailey, J. E., & Chescoe, D. (1979). Microstructure development during the hydration of portland cement. *Micron, 11*, 153–181.
Berodier E (2015) Impact of the Supplementary Cementitious Materials on the kinetics and microstructural development of cement hydration. PhD Thesis. 6417:154. https://infoscience.epfl.ch/record/204690/files/EPFL_TH6417.pdf%5Cnhttp://files/148/EPFL_TH6417.pdf
Bizzozero, J., Gosselin, C., & Scrivener, K. L. (2014). Expansion mechanisms in calcium aluminate and sulfoaluminate systems with calcium sulfate. *Cement and Concrete Research, 56*, 190–202. https://doi.org/10.1016/j.cemconres.2013.11.011
Chamrova, R. (2010). Modelling and measurement of elastic properties of hydrating cement paste. *EPFL., 4606*, 128.
De Weerdt, K., Lothenbach, B., & Geiker, M. R. (2019). Comparing chloride ingress from seawater and NaCl solution in Portland cement mortar. *Cement and Concrete Research, 1*(115), 80–89.
El-Didamony, H., Heikal, M., Moselhy, H., & Ali, M. A. (2016). Utilization of GBFS in the preparation of low cost cement. *Egyptian Journal of Chemistry, 59*(4), 623–636.
El-Dieb, A. S., Taha, M. R., & Abu-Eishah, S. I. (2019). The use of ceramic waste powder (CWP) in making eco-friendly concretes. In D. E. Quesada, L. P. Villarejo, & P. S. Soto (Eds.), *Ceramic materials-synthesis, characterization, applications and recycling.* London: IntechOpen. https://doi.org/10.5772/intechopen.81842
El-Gammal, M., Badr, E. S., Asker, S. A., Ibrahim, M. S., & Galad, N. M. (2011). Health risk assessment of marble dust at marble workshops. *Natural Science, 9*(11), 1545–1740.
Ergün, A. (2011). Effects of the usage of diatomite and waste marble powder as partial replacement of cement on the mechanical properties of concrete. *Construction and Building Materials, 25*(2), 806–812.
ESS 1109/2002. (2002) Egyptian standard specification, aggregate for concrete. p. 2002.
ESS 1658/2006 (2006) Egyptian standard specification "testing of concrete". 2006.
ESS 2421/2005. (2005) Egyptian standard specification cement-physical and mechanical tests. p. 2421.
European commission, health and consumer protection (2006) Targeted risk assessment report on sodium hydroxide (NaOH) environmental part. Environment. p. 2–7.
Fernández, Á., Lothenbach, B., Alonso, M. C., & García Calvo, J. L. (2018). Thermodynamic modelling of short and long term hydration of ternary binders. Influence of Portland cement composition and blast furnace slag content. *Construction and Building Materials, 166*, 510–521.
Galetakis, M., & Soultana, A. (2016). A review on the utilisation of quarry and ornamental stone industry fine by-products in the construction sector. *Construction and Building Materials, 102*, 769–781.

Gallucci, E., & Scrivener, K. (2007). Crystallisation of calcium hydroxide in early age model and ordinary cementitious systems. *Cement and Concrete Research, 37*(4), 492–501.
Ghrair, A. M., & Al-Mashaqbeh, O. (2016). Domestic wastewater reuse in concrete using bench-scale testing and full-scale implementation. *Water, 8*(9), 366.
Ghrair, A. M., Heath, A., Paine, K., & Kronz, A. M. (2020). Waste wash-water recycling in ready mix concrete plants. *Environment, 7*(12), 1–15.
Gudainiyan, J., & Kishore, K. (2023). A review on cement concrete strength incorporated with agricultural waste. *Materials Today: Proceedings*. https://doi.org/10.1016/j.matpr.2022.10.179
Jhatial, A. A., Nováková, I., & Gjerløw, E. (2023). A review on emerging cementitious materials, reactivity evaluation and treatment methods. *Buildings, 13*, 526. https://doi.org/10.3390/buildings13020526
Jiang, H., Qi, Z., Yilmaz, E., Han, J., Qiu, J., & Dong, C. (2019). Effectiveness of alkali-activated slag as alternative binder on workability and early age compressive strength of cemented paste backfills. *Construction and Building Materials, 218*, 689–700. https://doi.org/10.1016/j.conbuildmat.2019.05.162
Kulik, D. A., Wagner, T., Dmytrieva, S. V., Kosakowski, G., Hingerl, F. F., Chudnenko, K. V., et al. (2013). GEM-Selektor geochemical modeling package: Revised algorithm and GEMS3K numerical kernel for coupled simulation codes. *Computers & Geosciences, 17*(1), 1–24.
Kumar, A., Oey, T., Kim, S., Thomas, D., Badran, S., Li, J., et al. (2013). Simple methods to estimate the influence of limestone fillers on reaction and property evolution in cementitious materials. *Cement and Concrete Composites, 42*, 20–29.
Kumar, R., Goyal, S., & Srivastava, A. (2021). A comprehensive study on the influence of supplementary cementitious materials on physico-mechanical, microstructural and durability properties of low carbon cement composites. *Powder Technology, 394*, 645–668. https://doi.org/10.1016/j.powtec.2021.08.081
Kunther, W., Dai, Z., & Skibsted, J. (2016). Thermodynamic modeling of hydrated white Portland cement-metakaolin-limestone blends utilizing hydration kinetics from 29Si MAS NMR spectroscopy. *Cement and Concrete Research, 1*(86), 29–41.
L'Hôpital, E., Lothenbach, B., Kulik, D. A., & Scrivener, K. (2016). Influence of calcium to silica ratio on aluminium uptake in calcium silicate hydrate. *Cement and Concrete Research, 85*, 111–121. https://doi.org/10.1016/j.cemconres.2016.01.014
Lauermannová, A. M., Paterová, I., Patera, J., Skrbek, K., Jankovský, O., & Bartůněk, V. (2020). Hydrotalcites in construction materials. *Applied Sciences., 10*, 1–13.
Li, L. G., Huang, Z. H., Tan, Y. P., Kwan, A. K. H., & Chen, H. Y. (2019). Recycling of marble dust as paste replacement for improving strength, microstructure and eco-friendliness of mortar. *Journal of Cleaner Production, 10*(210), 55–65.
Liu, Y., Zhang, Z., Hou, G., & Yan, P. (2021). Preparation of sustainable and green cement-based composite binders with high-volume steel slag powder and ultrafine blast furnace slag powder. *Journal of Cleaner Production, 289*, 125133. https://doi.org/10.1016/j.jclepro.2020.125133
Lothenbach, B., Matschei, T., Möschner, G., & Glasser, F. P. (2008). Thermodynamic modelling of the effect of temperature on the hydration and porosity of Portland cement. *Cement and Concrete Research, 38*(1), 1–18.
Lothenbach, B., & Nonat, A. (2015). Calcium silicate hydrates: Solid and liquid phase composition. *Cement and Concrete Research, 78*, 57–70. https://doi.org/10.1016/j.cemconres.2015.03.019
Lothenbach, B., Scrivener, K., & Hooton, R. D. (2011). Supplementary cementitious materials. *Cement and Concrete Research., 41*, 1244–1256.
Lothenbach, B., & Zajac, M. (2019). Application of thermodynamic modelling to hydrated cements. *Cement and Concrete Research, 123*, 105779. https://doi.org/10.1016/j.cemconres.2019.105779
Mackie, A., Boilard, S., Walsh, M. E., & Lake, C. B. (2010). Physicochemical characterization of cement kiln dust for potential reuse in acidic wastewater treatment. *Journal of Hazardous Materials, 173*(1–3), 283–291.
McNeil, K., & Kang, T. H. K. (2013). Recycled Concrete Aggregates: A Review. *Int J Concr Struct Mater., 7*(1), 61–69.
Prentice, D. P., Walkley, B., Bernal, S. A., Bankhead, M., Hayes, M., & Provis, J. L. (2018). Thermodynamic modelling of BFS-PC cements under temperature conditions relevant to the geological disposal of nuclear wastes. *Cement and Concrete Research, 2019*(119), 21–35. https://doi.org/10.1016/j.cemconres.2019.02.005
Quennoz, A., & Scrivener, K. L. (2013). Interactions between alite and C3A-gypsum hydrations in model cements. *Cement and Concrete Research, 44*, 46–54. https://doi.org/10.1016/j.cemconres.2012.10.018
Roslan, N. H., Ismail, M., Abdul-Majid, Z., Ghoreishiamiri, S., & Muhammad, B. (2016). Performance of steel slag and steel sludge in concrete. *Construction and Building Materials, 104*, 16–24. https://doi.org/10.1016/j.conbuildmat.2015.12.008
Sadek, D. M., El-Attar, M. M., & Ali, A. M. (2017). Physico-mechanical and durability characteristics of concrete paving blocks incorporating cement kiln dust. *Construction and Building Materials, 30*(157), 300–312.
Scrivener, K. L. (2004). Backscattered electron imaging of cementitious microstructures: Understanding and quantification. *Cement and Concrete Composites, 26*(8), 935–945.
Shayan A, Ivanusec I (1989) Influence of NaOH on mechanical properties of cement paste and mortar with and without reactive aggregate. In: 8th International Conference on Alkali-Aggregate Reaction. Icaar. P. 715–720.
Shi, Z., & Lothenbach, B. (2019). The role of calcium on the formation of alkali-silica reaction products. *Cement and Concrete Research, 1*, 126.
Shi, Z., & Lothenbach, B. (2020). The combined effect of potassium, sodium and calcium on the formation of alkali-silica reaction products. *Cement and Concrete Research, 1*, 127.
Souza, A. T., Barbosa, T. F., Riccio, L. A., & Dos, S. W. J. (2020). Effect of limestone powder substitution on mechanical properties and durability of slender precast components of structural mortar. *Journal of Materials Research and Technology, 9*(1), 847–856. https://doi.org/10.1016/j.jmrt.2019.11.024
Taji, I., Ghorbani, S., de Brito, J., Tam, V. W. Y., Sharifi, S., Davoodi, A., et al. (2019). Application of statistical analysis to evaluate the corrosion resistance of steel rebars embedded in concrete with marble and granite waste dust. *Journal of Cleaner Production, 10*(210), 837–846.
Tugrul Tunc, E. (2019). Recycling of marble waste: A review based on strength of concrete containing marble waste. *Journal of Environmental Management., 231*, 86–97.
Tugrul Tunc, E., & Alyamac, K. E. (2020). Determination of the relationship between the Los Angeles abrasion values of aggregates and concrete strength using the Response Surface Methodology. *Construction and Building Materials, 260*, 119850. https://doi.org/10.1016/j.conbuildmat.2020.119850
Tugrul Tunc, E., & Esat, A. K. (2019). A preliminary estimation method of Los Angeles abrasion value of concrete aggregates. *Construction and Building Materials, 222*, 437–446. https://doi.org/10.1016/j.conbuildmat.2019.06.176
Vijayalakshmi, M., Sekar, A. S. S., & Ganesh, P. G. (2013). Strength and durability properties of concrete made with granite industry waste. *Construction and Building Materials, 46*, 1–7.
Vollpracht, A., Lothenbach, B., Snellings, R., & Haufe, J. (2016). The pore solution of blended cements: A review. *Mater Struct Constr., 49*(8), 3341–3367.
Wang, D., Shi, C., Farzadnia, N., Shi, Z., & Jia, H. (2018). A review on effects of limestone powder on the properties of concrete. *Construction and Building Materials, 192*, 153–166. https://doi.org/10.1016/j.conbuildmat.2018.10.119
Way, S. J., & Shayan, A. (1989). Early hydration of a Portland cement in water and sodium hydroxide solutions: Composition of solutions and nature of solid phases. *Cement and Concrete Research, 19*(5), 759–769.
Wu, M., Sui, S., Zhang, Y., Jia, Y., She, W., Liu, Z., et al. (2021). Analyzing the filler and activity effect of fly ash and slag on the early hydration of blended cement based on calorimetric test. *Construction and Building Materials, 276*, 122201. https://doi.org/10.1016/j.conbuildmat.2020.122201
Zajac, M., Skocek, J., Adu-Amankwah, S., Black, L., & Ben, H. M. (2018). Impact of microstructure on the performance of composite cements: Why higher total porosity can result in higher strength. *Cement and Concrete Composites, 1*(90), 178–192.

Publisher's Note

Springer Nature remains neutral with regard to jurisdictional claims in published maps and institutional affiliations.